Case Studies in Thermal Engineering 51 (2023) 103476

Contents lists available at ScienceDirect

Case Studies in Thermal Engineering

journal homepage: www.elsevier.com/locate/csite

Thermal performance of Oldroyd-B hybrid nanofluid in solar energy-based water pumping systems and entropy generation minimization

A.M. Obalalu [a], M. Asif Memon [b], S. Saleem [c], A. Abbas [d], O.A. Olayemi [e,f], Mohamed R. Ali [g,h,*], R. Sadat [i], A.S. Hendy [j]

[a] Department of Mathematical Sciences, Augustine University Ilara-Epe, Lagos, Nigeria
[b] Department of Mathematics and Social Sciences, Sukkur IBA University, Sukkur, 65200, Sindh, Pakistan
[c] Department of Mathematics, College of Science, King Khalid University, Abha, 61413, Saudi Arabia
[d] Department of Mathematics, Faculty of Science, University of Gujrat, Sub-Campus, Mandi Bahauddin 50400, Pakistan
[e] School of Engineering, Cranfield University, Cranfield, UK
[f] Department of Aeronautics and Astronautics, Faculty of Engineering and Technology, Kwara State University, Malete, Kwara State, Nigeria
[g] Faculty of Engineering and Technology, Future University in Egypt, New Cairo, 11835, Egypt
[h] Basic Engineering Science Department, Benha Faculty of Engineering, Benha University, Benha, Egypt
[i] Department of Mathematics, Zagazig Faculty of Engineering, Zagazig University, Egypt
[j] Department of Computational Mathematics and Computer Science, Institute of Natural Sciences and Mathematics, Ural Federal University, 19 Mira St., Yekaterinburg 620002, Russia

ARTICLE INFO

Handling Editor: Huihe Qiu

Keywords:
Solar water pumping (SWP)
Solar thermal energy
Galerkin weighted residual method
Aluminum alloy
Titanium alloy
Ethylene glycol

ABSTRACT

The growing need for reliable energy supply to enhance productivity in industrial and residential sectors underscores the importance of conserving solar energy. This can be achieved through measures such as optimizing solar collector coatings and optical heat processes. The environmental risks posed by fossil fuels, like coal and diesel, for electricity generation, further highlight the urgency of seeking alternative solutions. Solar energy has emerged as a highly promising option, capturing global attention for its potential to improve productivity and sustainability. The study focuses on examining aluminum alloy-titanium alloy/ethylene glycol hybrid nanofluid in the flow of non-Newtonian Oldroyd-B through a parabolic trough surface collector located in the solar water pumps (SWP). The Galerkin weighted residual method was utilized to solve the group of equations that describe momentum, energy, and entropy generation. The findings show that the hybrid nanofluid leads to better thermal radiative performance compared to the ordinary nanofluid. Therefore, the implications of these findings are substantial, particularly in the fields of thermal engineering and renewable energy. By offering insights into the efficient utilization of solar energy in water pumping systems and the reduction of entropy generation, this research has the potential to drive innovations that enhance the sustainability and performance of such systems.

* Corresponding author. Faculty of Engineering and Technology, Future University in Egypt, New Cairo, 11835, Egypt.
E-mail address: mohamed.reda@fue.edu.eg (M.R. Ali).

https://doi.org/10.1016/j.csite.2023.103476
Received 5 June 2023; Received in revised form 30 August 2023; Accepted 7 September 2023
Available online 22 September 2023

1. Introduction

In recent years, the escalating levels of worldwide carbon dioxide (CO_2) emissions have raised pressing concerns. These emissions have notably contributed to the ongoing climate change, leading to a spectrum of impacts on human life and the environment. This critical issue underscores the need for alternative energy sources that can mitigate CO_2 emissions. Among such sources, solar energy stands out due to its potential to supply clean power to both households and industries [1]. Solar technology stands as a prominent model of renewable energy, aligning seamlessly with the global objective to substantially reduce carbon emissions. By harnessing the sun's energy, it generates electricity without the concurrent release of carbon dioxide, making a pivotal contribution to environmental preservation. In a recent study by Alimonti et al. [2], it was highlighted that the integration of solar energy could potentially lead to a substantial 75% reduction in global carbon dioxide emissions by the year 2050. A study conducted by the US Department of Energy revealed that the sun's direct rays on the earth's surface for just an hour and a half can fulfill the energy requirements of the entire world for a year [3]. It is of utmost importance to minimize the worldwide emission of CO_2 to protect human life from the damaging consequences of climate change [4].

Two primary categories of accessible solar energy are photovoltaic (PV) and concentrated solar power (CSP). Photovoltaic (PV) technology involves the conversion of solar energy into electrical power through the use of semiconductors [5]. These PV cells, typically composed of silicon, are capable of releasing electrons upon exposure to sunlight, thereby generating direct current electricity [6]. This technology plays a pivotal role in harnessing solar energy for practical applications. PV systems can be utilized to power smaller devices such as calculators, garden lights, and phone chargers. Similarly, they can also be applied on a larger scale such as solar farms and also can generate a significant amount of electricity capable of powering entire cities or regions. CSP refers to a type of solar power technology that utilizes mirrors or lenses to concentrate sunlight on a small surface area. The concentrated solar energy is subsequently transformed into electricity through different mechanisms like photovoltaic cells, thermal heat engines, or thermoelectric generators [7]. According to the report of Ochoa et al. [8], desert regions like California and Arizona in the US have favorable climatic conditions for the development of larger plants that use concentrated solar power. Renewable energies are becoming increasingly important in mitigating the adverse effects of climate change. Among these sources, sun-based energy stands out as a preferred choice due to its renewability and lack of hazardous pollutant discharge [9]. Unlike fossil fuels, which contribute significantly to environmental pollution, solar energy offers a cleaner, more sustainable alternative that can meet our energy needs without harming our planet. Therefore, solar energy is a better option among other forms of energy due to its numerous environmental benefits and potential for long-term use.

The use of solar water pumps (SWP) in agriculture is an exciting area of research that combines renewable energy with sustainable farming practices. By harnessing the sun's power, SWPs enable farmers to efficiently irrigate their crops while also reducing greenhouse gas emissions [10]. To ensure optimal performance, it is crucial to operate SWPs within a suitable temperature range. SWPs are electrical systems that utilize one or more photovoltaic panels to generate electricity for pumping water. This innovative system offers a sustainable and eco-friendly solution for watering agricultural lands, livestock, and other purposes that require water pumping, without relying on traditional grid electricity [11]. By implementing SWPs, farmers can reduce their dependence on fossil fuels and contribute to a cleaner environment. These pumps not only provide a reliable and cost-effective method of water circulation but also offer long-term benefits in terms of energy efficiency and carbon footprint reduction. In addition to their environmental advantages, SWPs have the potential to improve the overall productivity of agricultural systems. They allow farmers to optimize water usage and effectively manage irrigation schedules, leading to healthier crops and increased yields. Furthermore, the use of SWPs can provide access to water resources in remote areas where grid electricity may not be readily available. This promotes inclusive and sustainable development by empowering farmers in such regions to enhance their farming capabilities and improve their livelihoods. The integration of SWPs into agricultural practices requires a comprehensive understanding of system design, installation, and maintenance. It is essential to ensure that these pumps are properly sized and located, taking into account factors such as solar radiation, water demand, and system efficiency. In conclusion, the use of solar water pumps in agriculture presents an innovative and sustainable approach to irrigation. By harnessing the power of the sun, these pumps offer numerous benefits, including increased efficiency, reduced greenhouse gas emissions, and enhanced agricultural productivity. Through further advancements in technology and continued research, SWPs have the potential to revolutionize farming practices and contribute to a greener future. In water supply systems, water is either pumped from underground or transported into a storage reservoir where it can be used for gravitational energy. Therefore, energy conservation measures are not necessary for these types of systems [12]. The device was responsible for regulating the solar pressure which is powered either by electricity harnessed from the photovoltaic array or through the absorption of radiant heat generated by solar light [13]. In 1883, Charles Fritts demonstrated the first practical use of photovoltaic cells to generate electricity for 15 homes using water pumps [14]. This indicated a significant milestone in the field of renewable energy and has paved the way for further developments in sustainable power generation. Meanwhile, since 1993, a large number of photovoltaic (PV) water pumps had been put into use worldwide. As reported via [15], stated that the number of these installations increased significantly and reached approximately 60,000 in 1998.

Parabolic Trough Solar Collection (PTSC) is an innovative technology harnessing concentrated sunlight for thermal energy production. It utilizes a parabolic trough reflector to focus sunlight onto a receiver tube, offering potential for enhanced efficiency [16]. Widely adopted in large-scale solar thermal power plants globally, PTSC's competitive edge among renewable sources prompts further research. Its ability to store thermal energy for use during sun-limited periods contributes to its value as a dependable renewable solution. As sustainable energy demand grows, PTSC's continuous operation and reliability make it a key player in the pursuit of cleaner energy alternatives [17,18]. The utility of PTSC is underscored by its capacity to operate efficiently in regions characterized by frequent cloud cover or restricted daylight duration. Consequently, PTSC emerges as a pivotal sustainable energy alternative.

Furthermore, the study conducted by Obalalu et al. [19] explores the possibility of increasing the mechanical energy of solar aircraft by using HNF on their aircraft wings. The researchers used PTCS as a method to achieve this objective and to demonstrate that renewable and sustainable energy sources can be successfully integrated into aviation technology. Overall, the study highlights the potential of using clean energy in aviation for a more environmentally friendly approach to air travel. According to Chandrasekaran et al. [20] the effectiveness of PTSC and thermal transport for hybrid nanofluid flow involving Sodium Alginate Water-Based Copper-Graphene Oxide, using the non-Newtonian Maxwell model across an expanding sheet surface of the solar aircraft wing [21].

The utilization of nanofluids (NF) as absorbers is a proactive method to improve the thermal efficiency of solar devices [22]. The thermophysical properties of nanofluids make them a promising option to improve solar devices, which can effectively enhance the efficiency of solar collectors according to previous studies [23,24]. NF is a promising solution for improving heat transfer performance in solar applications, as they possess remarkable thermal properties. The dispersed nanoparticles (NPs) possess a remarkable thermal conductivity which makes them capable of carrying heat along with them. This characteristic proves to be beneficial for utilizing solar energy and maintaining the temperature of PV cells at an optimal level [25]. Nanofluids are contained metal nanoparticles (NPs) (SiO2) Silicon dioxide, (Fe2O3) Iron (III) oxide or ferric oxide, (CuO) Copper (II) oxide, (ZnO) Zinc oxide, (TiO2) Titanium dioxide, (ZrO2) Zirconium dioxide, (Fe3O4) Iron (II, III) oxide or magnetite, (Al2O3) Aluminium oxide, and metal oxide NPs are Graphene, (CNT) Carbon nanotubes, and (SiO2) Silicon dioxide [26]. Nanofluids offer several benefits to solar energy systems, including enhanced heat transfer properties, decreased weight and size, improved stability, and reduced costs. The computational study for heat transport in hydrodynamic unsteady flow by applying copper-engine oil (Cu-EO) and silver-engine oil (Ag-EO) NF flowing in a sun-based tractor with thermal radiation effect was study by Ref. [27]. Waqas et al. [28] stated that the thermal distributions of (Copper Oxide/Water, Molybdenum Sulfide/Water, and Titanium Dioxide/Water) are improved as a result of an increase in the nano-metal-shaped factor. The MHD flow of time-fractional Casson nanofluid using generalized Fourier and Fick's laws over an inclined channel with applications of gold nanoparticles was examined in the study by Ref. [29]. Numerical analysis of newly developed fractal-fractional model of Casson fluid with exponential memory was examined in the study by Ref. [30]. Analysis and numerical simulation of fractal-fractional order non-linear couple stress nanofluid with cadmium telluride nanoparticles were investigated in a study conducted by Ref. [31]. Parametric simulation of hybrid nanofluid flow consisting of cobalt ferrite nanoparticles with second-order slip and variable viscosity over an extending surface was studied by Ref. [32].

The utilization of hybrid nanofluid (HNF) technology has received significant attention in recent years, and it is proving to be a groundbreaking solution for increasing the effectiveness of solar thermal collectors and photovoltaic cells [33]. HNFs are composite particles made up of two or more types of nanometer-sized materials functioning as nanoparticles. HNF can enhance heat transfer and light trapping efficiency, resulting in higher energy output. This is achieved by integrating nanoparticles with conventional heat transfer fluids [34]. Several scientific studies have previously explored the utilization of HNF as a heat transfer fluid in PTSC. These studies consider various nanoparticles, including silver (Ag)- copper oxide (CuO)/water (H2O) [35], magnetite (Fe3O4)-copper (Cu)/water (H2O) [36], aluminum oxide (Al2O3)-titanium dioxide (TiO2)/and Syltherm 800 [37]. Silver (Ag), magnesium oxide (MgO), and water (H2O) [38]. In summary, the effectiveness of a solar energy generation system heavily relies on the type and amount of HNF used. It is crucial to select an appropriate HNF that takes into account both its thermal and optical properties. In addition. This study of Copper (Cu) and Zirconium dioxide (ZrO2) HNF flow over a stretching sheet under slip conditions, and magnetic field effect were investigated by Ref. [39]. The numerical framework of alumina–copper/water HNF on non-Newtonian Powell-Eyring flow over a non-uniform stretching of the plate in the presence of suction/injection was studied by Ref. [40]. The features and aspects of radioactive flow and slippage velocity on rotating two-phase Prandtl nanofluid with zero mass fluxing and convective constraints were investigated in a study conducted by Ref. [41]. Thermal-enhanced hybrid of copper-zirconium dioxide/ethylene glycol nanofluid flowing in the solar collector of water-pump application was examined in the study by Ref. [42]. Thermal analysis characterization of solar-powered ship using Oldroyd hybrid nanofluids in parabolic trough solar collector were investigated in a study conducted by Ref. [43]. Irreversibility analysis of time-dependent magnetically driven flow of Sutterby hybrid nanofluid: a thermal mathematical model were investigated in a study conducted by Ref. [44]. The flow, thermal and mass properties of Soret-Dufour model of magnetized Maxwell nanofluid flow over a shrinkage inclined surface was examined in the study by Ref. [45]. Dynamics of ethylene glycol-based graphene and molybdenum disulfide hybrid nanofluid over a stretchable surface with slip conditions was examined in the study by Ref. [46]. Solar-HVAC thermal investigation utilizing (Cu-AA7075/C6H9NaO7) MHD-driven hybrid nanofluid rotating flow via second-order convergent technique: A novel engineering study were investigated in a study conducted by Ref. [47]. Quadratic multiple regression model and spectral relaxation approach for carreau nanofluid inclined magnetized dipole along stagnation point geometry was examined in the study by Ref. [48]. Thermal management of magnetohydrodynamic nanofluid within porous C-shaped cavity with undulated baffle was examined in the study by Ref. [49]. Thermal slip and homogeneous/heterogeneous reaction characteristics of second-grade fluid flow over an exponentially stretching sheet were investigated in a study conducted by Ref. [50].

Entropy generation is an important field of thermodynamics that refers to the gradual dissipation of energy within a system [51,52]. As solar energy becomes increasingly important, scientists are intensifying their efforts to comprehend the impact of entropy generation on this renewable resource. As we work towards a future that relies on solar energy for sustainability, investigating the mechanisms behind entropy generation can lead to new and creative methods for optimizing energy efficiency and reducing waste [53]. Bejan [54,55] investigated the creation of entropy and developed a method to optimize the efficiency of system destruction. Bejan's work presents a useful tool for engineers and scientists who are highly interested in studying entropy generation [56,57]. Shahzad et al. [58] conducted research that focused on the effectiveness of cooling an SWP using thermal energy. The study involves investigating the process of entropy generation and uses a novel kind of Buongiorno's model. The recent of work Obalalu et al. [59] focuses on entropy generation and hybrid nanofluids which were investigated through numerical simulations. Also, the study examines the potential application of carbon nanotubes in ethylene glycol as a working fluid.

1.1. The objective and novelty of the newly proposed model

As the entire world continues to face difficulties related to energy and the environment, there is an increasing desire for technological solutions that are both sustainable and efficient. Solar water pumps have found widespread use in a variety of applications, such as agriculture, the house, and market, and the care and feeding of livestock. This not only leads to elevated operational costs but also contributes to environmental issues such as increased emissions of greenhouse gases. The main novelty of the study is the investigation of the thermal performance of Oldroyd-B hybrid nanofluid in solar energy-based water pumping systems. Oldroyd-B hybrid nanofluid is a type of nanofluid that is made by dispersing two different types of nanoparticles in a base fluid. This type of nanofluid has been shown to have better thermal properties than traditional nanofluids, and it is therefore a promising contender for use in solar energy-based water pumping systems. Additionally, this study evaluates the effectiveness of a solar water pump in providing thermal cooling by making use of an HNF composed of (AA7075–EG, and AA7075–Ti–6Al–4V/EG). Also, this research investigates how the mono and hybrid nanofluids (PTSC) perform as coolant liquids for the SWP by studying their heat kinetics. The motivation for the study is to improve the efficiency of solar energy-based water pumping systems. Solar energy is a renewable and sustainable source of energy, but it is not always available. Water pumping systems that use solar energy can help to ensure a reliable supply of water, even when solar energy is not available. However, the efficiency of these systems can be limited by factors such as heat loss and entropy generation. The use of Oldroyd-B hybrid nanofluid can help to improve the efficiency of these systems by reducing heat loss and entropy generation. The research seeks to contribute to the optimization of renewable energy technologies and the advancement of sustainable engineering methodologies. Despite the importance of the work, it has not been previously published and the flow properties have not been examined before. The following are the study's aims:

- The goal is to examine how the hybrid nanofluid behaves under varying flow conditions in terms of heat transfer.
- Additionally, to examine how the concentration of nanoparticles affects both the thermal conductivity (the ability of a material to conduct heat) and viscosity (thickness or resistance to flow) of a given substance.
- This study investigates the impact of several factors such as heat generation, thermal radiation, viscous dissipation, porous materials, and thermal dissipation on heat exchange analysis.
- Furthermore, we want to measure the enhancements in the performance of a solar water pump when using a hybrid nanofluid instead of a traditional fluid.
- Finally, our objective is to optimize key design parameters for achieving the highest possible cooling efficiency in the solar water pump system.

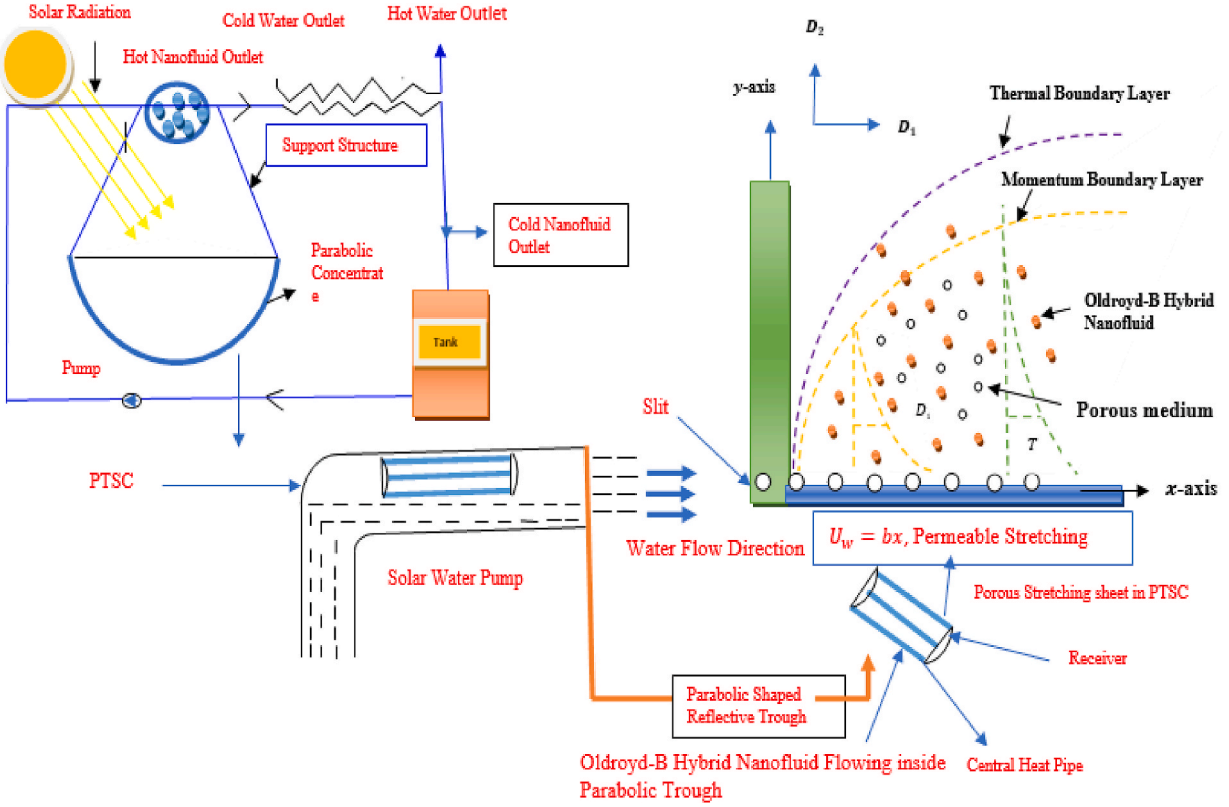

Fig. 1. Geometrical diagram of the flow model.

Achieving these goals can lead to the development of solar-powered water pumping systems that are more efficient and long-lasting, thereby contributing to solving issues related to energy and water security in remote areas.

Outline of current work.

The article is organized as follows: The mathematical and physical description of the problem is presented in the next section. The model of local Nusselt number is presented in section 3. Analysis of the entropy generation is presented in section 4. Section 5 deals with the concept of Galerkin weighted residual method and its application in solving the present nonlinear boundary value problems. In section 6, the obtained numerical results are presented graphically and discussed. Concluding remarks and future direction are given in the last section.

2. Mathematical and physical description

Suppositions and terms of the system: The conceptual foundation and limitations that are relevant to the flow model can be explained in the following manner:

- ❖ Slippery and convective boundary limitations.
- ❖ Two-dimensional laminar flow, Solar water pump
- ❖ Electromagnetic, heat generation, Thermal radiative flow
- ❖ Non-Newtonian Oldroyd-B fluid, Boundary-layer estimate
- ❖ Aluminum alloy, titanium alloy, and Ethylene glycol (EG) as Base fluid.
- ❖ Viscous dissipation, The second law of thermodynamics, Tiwari–Das model
- ❖ Different thermal conductivity, Porous medium

2.1. Flowing Geometric scheme

The equations of the mathematical flow model illustrated a horizontally moving plate through extended straight flat exterior with the U_w (x, 0) = bx, where b is a positive constant. The temperature of an insulated surface is denoted by T_w (x, t) = $T_\infty + b^* x$ and is assumed to remain constant at $x = 0$. The thermal variant rate is denoted as b^*, while T_w refers to the temperature of the wall and T_∞ represents the ambient temperature. It is assumed that the surface that the surface is characterized by both slipperiness and a temperature difference. The linear solar energy radiation takes place on the parabolic trough solar collector of the photovoltaic cells containing non-Newtonian hybrid nanofluid non-Newtonian Oldroyd-B. This model also being affected by viscous dissipation and heat sources. Fig. 1 displayed the SWP application modeling and geometric flowing diagram. The governing equations below (1–4) represent the viscous hybrid nano-fluid Oldroyd-B flow near the penetrable surface. This model also being affected by viscous dissipation and heat sources.

Governing Equations of the Physical Model: The equations that govern the HNF non-Newtonian Oldroyd-B flow model with magnetic field, heat generation, and thermal radiation can be expressed as follows [60]:

$$\frac{\partial D_1}{\partial x}+\frac{\partial D_2}{\partial y}=0 \tag{1}$$

$$D_1\frac{\partial D_1}{\partial x}+D_2\frac{\partial D_2}{\partial y}+\gamma_1\left(D_1{}^2\frac{\partial^2 D_1}{\partial x^2}+D_2{}^2\frac{\partial^2 D_1}{\partial y^2}+2D_1D_2\frac{\partial^2 D_1}{\partial x\partial y}\right)=\frac{\mu_{hnf}}{\rho_{hnf}}\left(\frac{\partial^2 D_1}{\partial y^2}\right)-\frac{\sigma_{hnf}B_0^2}{\rho_{hnf}}D_1-\frac{\mu_{hnf}}{\rho_{hnf}}\left(\frac{A_2}{k}\right)$$
$$+\frac{\mu_{hnf}}{\rho_{hnf}}\left(\gamma_2\left(D_1\left(\frac{\partial^3 D_1}{\partial x\partial y^2}\right)-\frac{\partial D_1}{\partial x}\left(\frac{\partial^2 D_1}{\partial y^2}\right)+\frac{\partial D_2}{\partial y}\left(\frac{\partial^2 D_1}{\partial y^2}\right)+D_2\left(\frac{\partial^3 D_1}{\partial y^3}\right)\right)\right), \tag{2}$$

$$D_1\frac{\partial T}{\partial x}+D_2\frac{\partial T}{\partial y}=\frac{k_{hnf}}{(\rho C_p)_{hnf}}\left(\frac{\partial^2 T}{\partial y^2}\right)+\frac{1}{(\rho C_p)_{hnf}}Q(T-T_w)+\frac{\mu_{hnf}}{(\rho C_p)_{hnf}}\left(\frac{\partial D_1}{\partial x}\right)^2-\frac{1}{(\rho C_p)_{hnf}}\left(\frac{\partial q_r}{\partial y}\right)+\frac{\sigma_{hnf}B_0^2}{(\rho C_p)_{hnf}}D_1^2, \tag{3}$$

with boundary conditions [47]:

Table 1
Thermophysical properties of Nanofluid and Hybrid nanofluid.

Aspects	*Nanofluid*	*Hybrid nanofluid*
Viscosity	$\mu_{nf}=\frac{\mu_f}{(1-\varphi)^{2.5}}$	$\mu_{hnf}=\mu_f/(1-(\varphi_1+\varphi_2))^{2.5}$
Density	$\rho_{nf}=(1-\varphi)\rho_f-\varphi\rho_s$	$\rho_{hnf}=(1-(\varphi_1+\varphi_2))\rho_f+\varphi_1\rho_{s_1}+\varphi_2\rho_{s_2}$
Heat capacity	$(\rho C_p)_{nf}=(1-\varphi)(\rho C_p)_f-\varphi\,(\rho C_p)_s$	$(\rho C_p)_{hnf}=(1-(\varphi_1+\varphi_2))(\rho C_p)_f+\varphi_1(\rho C_p)_{s1}+\varphi_2(\rho C_p)_{s2}$
Thermal conductivity	$\frac{k_{hnf}}{k_{gf}}=\frac{(k_s+2k_f)-2\varphi(k_f-k_s)}{(k_s+2k_f)+\varphi(k_f-k_s)}$	$\frac{k_{hnf}}{k_{nf}}=\left(\frac{(k_{s2}+2k_{nf}-2\varphi_2(k_{nf}-k_{s2})}{(k_{s2}+2k_{nf}+\varphi_2(k_{nf}-k_{s2})}\right)$
		$\frac{k_{nf}}{k_f}=\left(\frac{k_{s1}+2k_f-2\varphi_1(k_f-k_{s1})}{(k_{s1}+2k_f+\varphi_1(k_f-k_{s1})}\right)$

$$D_1(x,0) = U_w + M_w\left(\frac{\partial D_1}{\partial y}\right),$$
$$D_2(x,0) = P_w, \tag{4}$$
$$-k_O\left(\frac{\partial T}{\partial y}\right) = h_g(T_w - T), D_1 \longrightarrow 0, \frac{\partial D_1}{\partial y} \longrightarrow 0, T \longrightarrow T_\infty, as \quad y \longrightarrow \infty.$$

Table 2 contains information regarding the thermo-physical properties of the nanofluid and the corresponding symbols that were utilized in this study (see Table 1). To fully study the behavior of heated surfaces, physical parameters must be considered. However, this includes understanding how they release heat through conduction (also known as Newtonian heating) and how the liquid on the surface impacts the velocity of the liquid particles around it (known as slip condition). Two nanoparticles: Aluminum alloy (AA7075) and Titanium alloy (Ti-6Al-4 V) were added to ethylene glycol (EG) standard base fluid, each of them as a concentration factor size φ_{AA7075} and $\varphi_{Ti-6Al-4\ V}$.

Futures of nanofluid and hybrid nanofluid: The use of hybrid nanofluids involves combining nanoparticles with a base fluid. By immersing this mixture into an ordinary fluid, the heat transfer rate can be improved due to its ability to supply more heat. Table 2 summarizes the variables for Oldroyd-B hybrid nanofluids, with further details available in Refs. [2,3].

Nanoparticle features and Basefluid: The Physical aspects of Ti-6Al-4V (titanium alloy), AA7075 (aluminum alloy), and ***Basefluid*** Ethylene glycol (EG) are display in Ref. [61].

In recent years, research has been conducted to investigate how the use of nanomaterials might enhance the performance of heat exchangers [56]. Scientists have identified titanium alloys are nanomaterials with the potential to improve the efficiency of heat transmission in heat exchangers. A titanium alloy is a metallic material that is mainly composed of pure titanium and other elements or metals. The production process involves a meticulous combination of the titanium with different materials and cooling the mixture after obtaining the right proportions [62]. Titanium alloys find wide applications in hydrometallurgical, aerospace, and marine industries. Aluminium is a highly favored metal in the manufacturing industry due to its lightweight and impressive strength-to-weight ratio [63]. Manufacturers combine aluminum with other elements to create materials that possess distinctive characteristics suitable for specific industries. Ethylene glycol has gained significant attention in recent years due to its potential as a useful chemical for fuel enhancement and hydrogen gas transportation [62]. Due to their special qualities, such as high catalytic activity, selectivity, and stability under difficult reaction circumstances, titanium alloys have been investigated as prospective catalysts for the synthesis of EG. Solar water pumps have been created to utilize solar energy to pump water and are employed in a variety of fields, including water supply, livestock watering, and domestic water delivery in locations that do not have access to electricity. Solar water pumps can also be used in places where there is no access to electricity. The use of ethylene glycol synthesis catalysts made from titanium alloy could make solar water pumps more efficient and cost-effective. The new catalysts might make the manufacturing process for ethylene glycol more effective, and by reducing the production cost of materials used in solar water pumps. This, in turn, could lead to more people using this technology as it becomes more affordable, resulting in widespread adoption of this innovation.

Roseland Approximation (RA): This mathematical representation of RA in written form [64,65]:

$$qr = -\frac{4\sigma^*}{3k^*}\frac{\partial T}{\partial y} \tag{5}$$

Here, k* is the absorption coefficient, and σ* denotes the Stefan Boltzmann constant.

***Model solving*:** In the research on similarity technology, which converts the governing PDEs into ODEs, some modifications were made to the BVP formulas (1)-(4). Specifically, these adjustments involved incorporating the stream function and similarity quantities into the formula.

$$D_1 = \frac{\partial \psi}{\partial y}, and\ D_2 = -\frac{\partial \psi}{\partial x}, \tag{6}$$

and

$$\Gamma(x,y) = \sqrt{\frac{b}{\upsilon_f(1-\Gamma t)}}y,$$

$$\theta(\Gamma) = \frac{T - T_\infty}{T - T_\infty},$$

Table 2
The thermophysical factors of the of Ti-6Al-4V, and AA7075 nanoparticles, and EG base fluid [58].

Thermophysical	$\rho\ (kg/m^3)$	$C_p\ (J/kgK)$	$k\ (W/mK)$
Ti-6Al-4V (titanium alloy)	4420	0.56	7.2
AA7075 (aluminum alloy)	2810	960	173
Ethylene glycol (EG)	1114	2415	0.252

and $\psi(x,y)=\sqrt{\frac{v_f b}{(1-\Gamma t),}}xf(\Gamma)$

We derived the following equation.

$$f'''+\omega_1\omega_2\left(ff''-f'^2\right)-\frac{1}{\omega_1}\,Kf'+\omega_1\omega_2(2\varrho_1 ff')+\varrho_2 f''^2+\omega_1\omega_2\left(\varrho_1 f^2 f'''\right)-\varrho_2 ff''''=0, \tag{7}$$

$$\theta''\left(1+\frac{1}{\omega_4}N_r P_r\right)+\frac{\omega_3}{\omega_2}P_r f\theta'-\frac{\omega_3}{\omega_2}P_r f\theta'+\frac{1}{\omega_4}\,P_r Q\,\theta+\frac{1}{\omega_1\omega_3}P_r Ec f''^2=0, \tag{8}$$

Subjected to

$$f(0)=S, f'(0)=1+\delta f''(0), \theta'(0)=-B_i(1-\theta(0)), \text{as } f'(\Gamma)\longrightarrow 0, f'(\Gamma)\longrightarrow 0, \theta(\Gamma)\longrightarrow 0, \Gamma\longrightarrow\infty.. \tag{9}$$

where

$$\omega_1=(1-(\varphi_1+\varphi_2))^{2.5}, \omega_2=(1-(\varphi_1+\varphi_2))+\varphi_1\rho_{s_1}/\rho_f+\varphi_2\rho_{s_2}/\rho_f, \omega_3=(1-(\varphi_1+\varphi_2))+\varphi_1\left(\rho C_p\right)_{s1}/\left(\rho C_p\right)_f$$
$$+\varphi_2\left(\rho C_p\right)_{s2}/\left(\rho C_p\right)_f, \omega_4=\left(\frac{\left(k_{s2}+2k_{nf}-2\varphi_2\left(k_{nf}-k_{s2}\right)\right)}{\left(k_{s2}+2k_{nf}+\varphi_2\left(k_{nf}-k_{s2}\right)\right)}\right)\times\left(\frac{k_{s1}+2k_f-2\varphi_1\left(k_f-k_{s1}\right)}{\left(k_{s1}+2k_f+\varphi_1\left(k_f-k_{s1}\right)\right)}\right).$$

2.2. Description of the important symbols and expressions

The thermophysical attributes of Oldroyd-B hybrid nano-fluid and the Symbols with the governing equation employed in the present study are detailed in Table 3.

3. Modeling of local Nusselt number

This section explains important physical properties relevant to engineering, specifically to the proposed viscous hybrid nanofluid Oldroyd-B flow. The local Nusslet number (Nu_x) is a way to measure how quickly heat is being transferred in a system. Additionally, It's also defined as the rate of heat transfer. The Nu_x can be written as [66,67]:

$$Nu_x=\frac{xq_w}{k_f(T_w-T_\infty)}, \tag{10}$$

by applying dimensionless conversions to the aforementioned formula, becomes:

$$Nu_x Re_x^{1/2}=-\frac{k_{hnf}}{k_f}((1+N_r)\theta'(0)) \tag{11}$$

Table 3
Display the Symbols and description in the governing equation.

Parameters	Formula	Parameters	values
Thermal radiation parameter	$N_r=\frac{16}{3}\frac{\sigma^* T_\infty^3}{k^* v_f(\rho C_p)_f}$	Slip length	P_w
Deborah number I	$\varrho_1=b\,\gamma_1$	Velocity component	D_1, D_2
Biot number	$B_i=\frac{h_f}{k_o}\sqrt{\frac{v_f}{b}}$	Dynamic viscosity	μ_{hnf}
Deborah number II	$\varrho_2=b\,\gamma_2$	thermal conductivity of solid	k_O
Suction/Injection Parameter	$S=-P_w\sqrt{\frac{1}{v_f b}}$	heat transfer coefficient	h_g
Prandtl number	$P_r=\frac{v_f}{\alpha_f}$	Surface permeability	M_w
Porous medium	$K=\frac{v_f}{bk}$	Electrical conductivity	σ_{hnf}
local Nusselt Number	$Nu_x=\frac{xq_w}{k_f(T_w-T_\infty)},$	Particles	s
Eckert number	$Ec=\frac{U_w^2}{(C_p)_f(T_w-T_\infty)}$	Deborah number I, II	γ_1,γ_2
velocity slip	$\delta=\sqrt{\frac{b}{\mu_f}}M_w$	Specific heat	ρC_p
heat generation parameters	$Q=\frac{Q_0}{(\rho C_p)_f b}$	Thermal conductance	k_{hnf}

here $q_w = -k_{hnf}\frac{16}{3}\frac{\sigma^* T_\infty^3}{k^* v_f (\rho C_p)_f}\left(\frac{\partial T}{\partial y}\right)$, and $Re_x = \frac{U_w x}{v_f}$. Local Reynolds number is denoted as $Re_x = \frac{U_w x}{v_f}$.

4. Analysis of the entropy generation (Ng)

To properly use solar energy, it is crucial to have an understanding of the principles of thermodynamics, particularly the first and second laws. According to K. Loganathan and S. Rajan [68], entropy refers to the disruption of a system that is normally operating smoothly and the measurement of its irreversibility when it is enclosed. It is challenging to convert all of the sun's radiation into heat due to the presence of irreversibility, resulting in a decrease in the amount of work that can be produced from solar energy. In this research, we observed the generation of entropy caused by heat transfer and friction in nanofluids. We modified the formula for calculating entropy based on previous studies cited in Ref. [69].

$$E_G = \frac{k_{hnf}}{T_\infty^2}\left[\frac{16}{3}\frac{\sigma^* T_\infty^3}{k^* v_f (\rho C_p)_f} + \left(\frac{\partial D_1}{\partial y}\right)^2\right] + \frac{\mu_{hnf} v_1^2}{k T_\infty} + \frac{\mu_{hnf}}{T_\infty}\left(\frac{\partial v_1}{\partial y}\right)^2 \tag{12}$$

To simplify the calculation of Ng in equation (12), the dimensionless equation of entropy production is obtained as:

$$\mathrm{NG} = Re\omega_d(1-Nr)\theta'^2 + \frac{1}{\omega_1}\frac{Br}{\Omega}Re\left(Kf'^2 + f''^2\right) \tag{13}$$

5. Application of Galerkin-weighted residual method (GWRM)

The Galerkin-weighted residual method is a numerical scheme used to solve PDEs through the use of weighted residuals. This numerical scheme exhibits highly valuable in tackling problems BCs, which may pose a challenge for another numerical scheme. Here are the important steps that the Galerkin-weighted residual method involves:

The first step is to analyze formula (7)-(8):

$$f''' + \omega_1\omega_2\left(ff'' - f'^2\right) - \frac{1}{\omega_1}Kf' + \omega_1\omega_2(2\varrho_1 ff') + \varrho_2 f''^2 + \omega_1\omega_2\left(\varrho_1 f^2 f'''\right) - \varrho_2 ff''' = 0, \tag{14}$$

$$\theta''\left(1 + \frac{1}{\omega_4}N_r P_r\right) + \frac{\omega_3}{\omega_2}P_r f\theta' - \frac{\omega_3}{\omega_2}P_r f\theta' + \frac{1}{\omega_4}P_r Q\,\theta + \frac{1}{\omega_1\omega_3}P_r Ecf''^2 = 0, \tag{15}$$

In Step two, the Galerkin-weighted residual method employ a particular trail function to simulate the numeric outcome of formula (7)-(8), which can be examined as follows.

$$\begin{aligned}\widetilde{f}(\Gamma) &= s + s_1 e^{-\frac{\Gamma}{4}} + s_2 e^{-\frac{\Gamma}{2}} + \bullet\bullet\bullet\bullet\bullet\bullet\bullet\bullet\bullet\bullet\bullet\bullet\bullet\bullet\bullet\bullet\bullet\bullet + s_n e^{-\frac{n\Gamma}{3}} = \sum_{j=0}^{n} s_j e^{-\frac{i\Gamma}{4}},\\ \widetilde{\theta}(\Gamma) &= T_0 + T_1 e^{-\frac{\eta}{4}} + T_2 e^{-\frac{\eta}{2}} + \bullet\bullet\bullet\bullet\bullet\bullet\bullet\bullet\bullet\bullet\bullet\bullet\bullet\bullet\bullet\bullet\bullet\bullet + T_n e^{-\frac{m\eta}{3}} = \sum_{j=0}^{n} T_j e^{-\frac{i\Gamma}{4}},\end{aligned} \tag{16}$$

In the fourth step, residual vectors are produced for velocity and temperature by using the reduced trial solutions (33) and applying them to the method described in step one.

$$\begin{aligned}&\left(\sum_{j=0}^{n} s_j e^{-\frac{j\Gamma}{4}} - S\right)_{\eta=0} = 0, \left(\frac{\mathrm{d}}{\mathrm{d}\Gamma}\sum_{j=0}^{n} s_j e^{-\frac{j\Gamma}{4}} - 1 - \frac{\mathrm{d}^2}{d^2\eta}\sum_{j=0}^{n} s_j e^{-\frac{j\Gamma}{4}}\right)_{\Gamma=0} = 0\\ &\left(\frac{\mathrm{d}}{\mathrm{d}\Gamma}\sum_{i=0}^{n} \mathrm{T}_i e^{-\frac{j\eta}{4}} + B_i\left(1 + \sum_{i=0}^{n} \mathrm{T}_i e^{-\frac{j\eta}{4}}\right)\right)_{\Gamma=0} = 0\end{aligned} \tag{17}$$

In Step three, the procedure involves ensuring that the BCs for the problem the boundary conditions of formula (16) are satisfied via employing the trial solutions for the GWRM, which are**:**

$$R_f = \widetilde{f}''' + \omega_1\omega_2\left(\widetilde{f}\widetilde{f}'' - \widetilde{f}'^2\right) - \frac{1}{\omega_1}K\widetilde{f}' + \omega_1\omega_2(2\varrho_1\widetilde{f}\widetilde{f}') + \varrho_2\widetilde{f}''\widetilde{f}'^2 + \omega_1\omega_2\left(2\varrho_1\widetilde{f}^2\widetilde{f}'''\right)\varrho_2\widetilde{f}''\widetilde{f}'^2 = 0, \cong 0 \tag{18}$$

$$\boldsymbol{R}_\theta = \widetilde{\theta}''\left(1 + \frac{1}{\omega_4}N_r P_r\right) - \frac{\omega_3}{\omega_2}P_r(\widetilde{f}\widetilde{\theta}') - \frac{1}{\omega_1}P_r Q\widetilde{\theta}' + \omega_1\omega_2(2\varrho_1\widetilde{f}\widetilde{f}') + \frac{1}{\omega_1\omega_3}P_r Ecf''^2\widetilde{f}''^2\,\varrho_2\widetilde{f}\widetilde{f}''' = 0, \cong 0 \tag{19}$$

Step 5 Now, to examine the constants, the residual must be zero over the domain that is given below:

$$\int_0^{\infty} R_f e^{-\frac{j\Gamma}{4}} d\Gamma \approx \sum_{k=1}^{j}\left[A_k\left(e^{\Gamma} R_f e^{-\frac{j\Gamma}{4}}\right)_{\eta=x_k}\right]=0, \int_0^{\infty} R_\theta e^{-\frac{j\Gamma}{4}} d\Gamma \approx \sum_{k=1}^{j}\left[A_k\left(e^{\Gamma} R_\theta e^{-\frac{j\Gamma}{4}}\right)_{\eta=x_k}\right], =0, For\ j=0,1,2,\ldots,N-2, l=0,1,2,\ldots,N-2\ to\ zero. \tag{20}$$

Where A_k is described as:

$$A_k=\frac{1}{L_j'(x_k)}\int_0^{\infty}\frac{L_j(x)e^{-x}}{x-x_k}dx=\frac{(j!)^2}{x_k\left(L_j'(x_k)\right)^2}, L_j=e^x\frac{d^j}{dx^j}\left(e^{-x}x^j\right) \tag{21}$$

To minimize the residual errors, the weight functions $R_f e^{-\frac{j\Gamma}{4}}$, and $R_\theta e^{-\frac{j\Gamma}{4}}$ and residues product were integrated. A symbolic package MATHEMATICA was then utilized to calculate the unknown coefficients, and Fig. 2 illustrates the Galerkin-weighted residual method flow chart. In addition, the method's convergence is proven for the orders of approximation listed in Table 4. As display in Table 5, there was a strong correlation between the outcomes that previous published and the present findings

6. Discussion of results

This particular section deals with the investigation of the influences of several control parameters on the velocity flow $f'(\Gamma)$, thermal distribution $\theta(\Gamma)$, and entropy generation (Ng) are shown graphically. The ranges of control parameters are: Deborah number I (ϱ_1) and Deborah number II (ϱ_2), Thermal radiation (Nr = 1, 2, 3), Eckert number (Ec = 1, 2, 3), suction (S > 0), and injection (S < 0) heat generation (Q = 1, 2, 5) ($\delta = 0.1, 0.2, 0.4$), Biot number (Bi = 0.2, 2.0, ∞), nanoparticle volume friction ($\varphi, \varphi_h = 0.02, 0.06, 0.1$), Porous medium (K = 0.1, 0.6, 1.6), velocity sli p ($\delta = 0.1, 0.2, 0.4$), Reynolds number (Re 5,10,15), and Brinkman number (Br = 0.1,0.2,0. 3). Table 3 exhibits the Nusselt number for AA7075-Ti-6Al-4 V/ethylene glycol HNF and AA7075-ethylene glycol NF. As seen in Table 3, a faster rate of heat transfer contributes to an improvement in the efficiency and productivity of the thermal system. It has been demonstrated that this improvement has an advantageous influence on the thermal cooling of a solar water pump. The relative percentage of the smallest amount of Nr is displayed at the point of 43.3%, while the relative percentage of the greatest value of Nr is displayed at the point of 43.9%. In addition, Table 4 reveals a constant rate of thermal transmission for AA7075-Ti-6Al-4 V/ethylene glycol HNF and AA7075-ethylene glycol NF. As a result, it is appropriate to forecast an improvement in the overall performance of the thermal cooling of a solar water pump. It was revealed that the lowest and highest relative percentages for the AA7075-Ti-6Al-4 V/ethylene glycol HNF and AA7075-ethylene glycol NF were between 42.5% and 46.5% when the Ec was enhanced. The comparative percentage of the lowest value of ϱ_1 is shown at point 43.6%, while the comparative percentage of the highest value of ϱ_1 is shown at

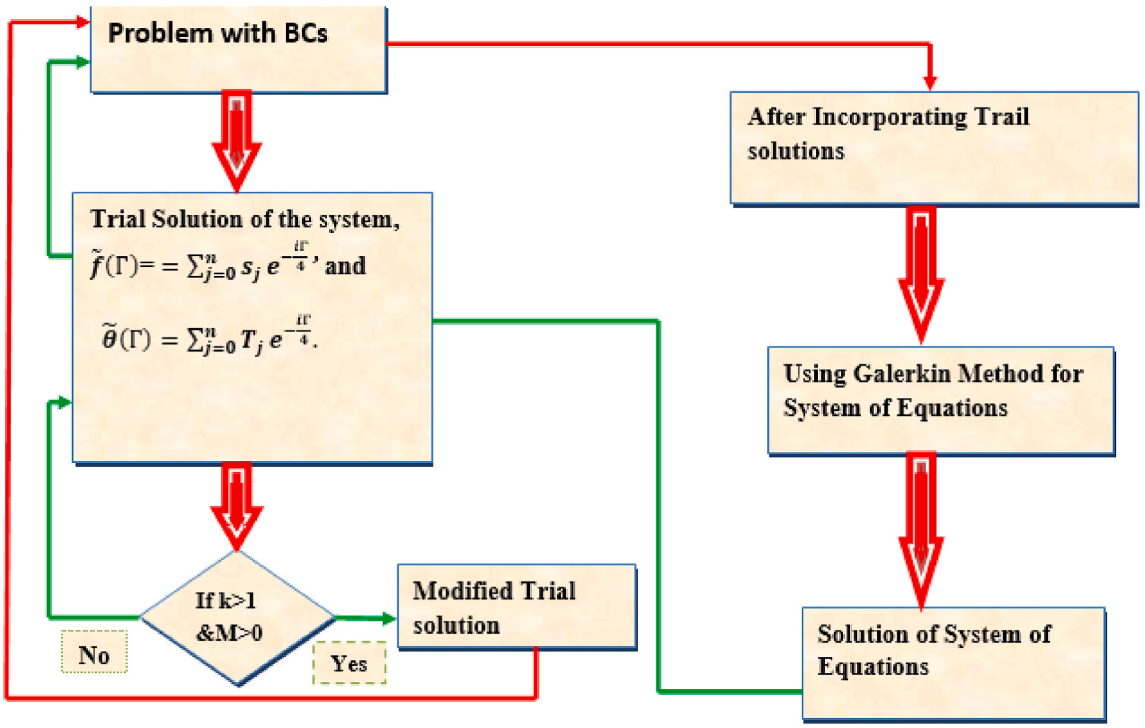

Fig. 2. The GWRM flow chart.

Table 4
Various approximation orders of convergence for Galerkin-weighted residual method solutions when Ec = N_r = 0.1, $\varrho_1 = \varrho_2$ = 0.2, Pr = 6.8.

Number of iteration (N)	$f'(\eta)$	$\theta'(\eta)$
4	1.0241	2.4486
6	1.1312	2.5231
8	1.2542	2.5231
10	1.2744	2.5231
12	1.2744	1.2093
14	1.2744	1.2093
16	1.2744	1.2093
20	1.2744	1.2093
24	1.2744	1.2093
30	1.2744	1.2093

Table 5
Comparison of heat transfer rate (Nu_x) for varying value of the Prandtl number (Pr).

Pr	Present outcome	The outcomes of [70]	The outcomes of [71]	The outcomes of [72]	The outcomes of [73]
0.72	0.8086	0.80863135	0.80876122	0.8086	0.80876181
1.0	1.0000	1.00000000	1.00000000	1.0000	1.00000000
3.0	1.9237	1.92368259	1.92357431	1.9236	1.92357420
7.0	3.0723	3.07225021	3.07314679	3.0723	3.07314651
10	3.7207	3.72067390	3.72055436	3.7006	3.72055429

Table 6
Value of Nusslet number (Nu_x) for AA7075-Ti-6Al-4 V/ethylene glycol HNF and AA7075- ethylene glycol NF.

Ec	N_r	ϱ_1	ϱ_2	φ, φ_h	Nu_x AA7075- EG	Nu_x AA7075-Ti-6Al-4 V/EG	Relative $\frac{Nu_{AA7075-Ti-6Al-4\ V/\ EG} - Nu_{AA7075-EG}}{Nu_{AA7075-Ti-6Al-4\ V/\ EG}} \times 100$
1	0.2	0.5	0.2	0.02	1.2238	2.1291	42.5%
3	0.2	0.5	0.2	0.02	1.2476	2.2425	44.4%
5	0.2	0.5	0.2	0.02	1.2589	2.3556	46.5%
1	**0.2**	0.5	0.2	0.02	1.2626	2.2264	43.3%
1	**0.3**	0.5	0.2	0.02	1.2659	2.2477	43.7%
1	**0.4**	0.5	0.2	0.02	1.2689	2.2631	43.9%
1	0.2	**0.1**	0.2	0.02	1.4154	2.5121	43.6%
1	0.2	**0.3**	0.2	0.02	1.4177	2.5187	43.7%
1	0.2	**0.5**	0.2	0.02	1.4193	2.5232	43.8%
1	0.2	0.5	**0.1**	0.02	1.4160	2.5129	43.6%
1	0.2	0.5	**0.2**	0.02	1.4180	2.5191	43.7%
1	0.2	0.5	**0.5**	0.02	1.4199	2.5239	43.8%
1	0.2	0.5	0.2	**0.01**	1.7822	2.5133	29.1%
1	0.2	0.5	0.2	**0.3**	1.7834	2.5253	29.4%
1	0.2	0.5	0.2	**0.5**	1.7841	2.2297	29.5%

point 43.8%. It was revealed that the least and highest relative percentages for the AA7075-Ti-6Al-4 V/ethylene glycol HNF and AA7075-ethylene glycol NF were between 42.5% and 46.5% when the φ, φ_h was increased. During the Thermal cooling process, it is preferable to make use of HNF to improve the mechanical properties of the solar water pump. Furthermore, the thermal conductivity of the Nu_x increases as the φ, φ_h get larger (Table 6).

6.1. Effect of thermal radiation parameter on $\boldsymbol{\theta}(\boldsymbol{\Gamma})$, and Ng for to (AA7075-Ti-6Al-4 V/ethylene glycol) HNF and (AA7075- ethylene glycol) NF

The impact of thermal radiation is substantial as it plays a crucial role in regulating the temperature of the Earth. This involves maintaining an equilibrium between the incoming solar radiations and the outgoing thermal radiation from the Earth, which helps to balance out any heat differences. Energy is released by radiation as electrically charged particles or waves that have the potential to ionize and have high energies. Radiation can come from several sources in fluid systems, including contamination by radioactive materials, radiation absorption by the fluid itself, and heat transfer between heated surfaces and the fluid. Fig. 3a displays a temperature profile that has been improved, showing higher (N_r) values ranging from 1 to 200. When compared to (AA7075-Ti-6Al-4 V/ethylene glycol), the physical characteristics of (AA7075- ethylene glycol) lead to a smaller temperature variation value. Based on our findings, increasing thermal radiation has a positive effect on the thermal gradient. In particular, higher values of the thermal radiation parameter result in a decrease in the mean absorption coefficient and an overall improvement in the thermal field. Thermal radiation can effectively elevate the temperature of nanofluids, and the sun is a great source of this radiation. N_r heat enhances both the fluid temperature and the temperature field by allowing the flow of fluid through the system. The thermal efficiency of the system will be

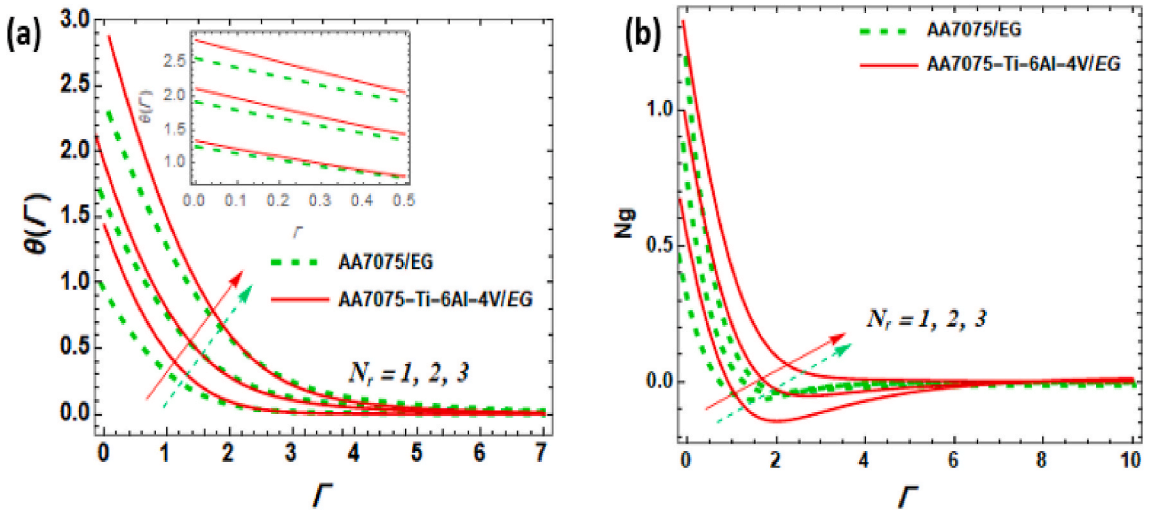

Fig. 3. Effect of N_r on $\theta(\Gamma)$, and Ng.

enhanced as a result of this occurrence. The use of physically generated thermal radiation is important in a variety of industries, including combustion reactors, polymer manufacturing, pasteurization, and waste disposal, because it boosts the heat transfer rate of fluids. The behavior of the entropy generation via the impact of N_r is displayed in Fig. 3b. The N_r increased the Entropy to enhance the thermal radiative. The occurrence of this phenomenon can be attributed to the irreversible nature of heat transfer happening within the system. It was observed that the physical characteristics (AA7075-Ti-6Al-4 V/ethylene glycol) HNF is higher than the (AA7075-ethylene glycol) NF.

6.2. *Effect of Eckert number (Ec) and heat generation (Q) on $\theta(\Gamma)$, and Ng for to (AA7075-Ti-6Al-4 V/ethylene glycol) HNF and (AA7075- ethylene glycol) NF*

The Eckert number (Ec) is a non-dimensional quantity employed in the field of fluid mechanics for quantifying the relative significance of kinetic energy over thermal energy in the flow of a fluid. Specifically, it represents the ratio between the convective term of kinetic energy and enthalpy. The term Ec holds great importance in the field of continuum mechanics and plays a vital role in its study. The findings indicate that the propagation of heat is notably amplified in the case of Ec, and there is a significant rise in the thickness of the thermal boundary layer. Consequently, the enhancement of (AA7075-Ti-6Al-4 V/ethylene glycol) is larger than NF of (AA7075-ethylene glycol). The Eckert number is used to characterize the mechanism of transforming kinetic energy into internal energy in a viscous fluid by applying work in the opposite direction. Raising the Eckert number amplifies the conversion of kinetic energy into thermal energy, giving rise to convective mixing and augmenting heat transfer proficiency in nanofluids Fig. 4a. Hence, examining the Eckert number is essential for comprehending and refining thermal control mechanisms in different sectors of engineering such as electronics cooling, aerospace, and automotive industries. Hence, when there is more heat dissipation due to viscosity, it results in both higher temperature and increased movement. It should be emphasized that the lack of consideration for this phenomenon is a contributing factor to the overestimation of high temperatures in some weak thermo-magnetic simulations. As a result of increased

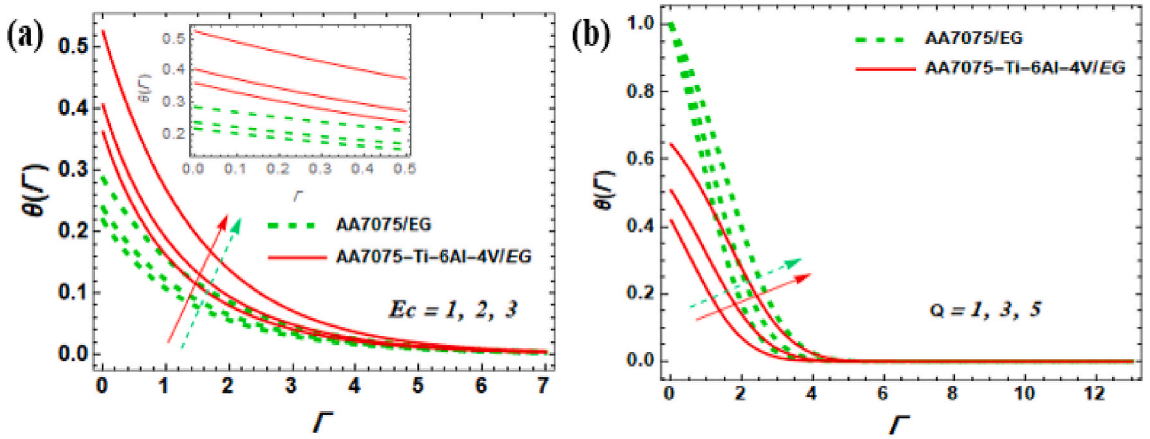

Fig. 4. Impact of *Ec and* Q on $\theta(\Gamma)$, and Ng.

viscosity, more heat is dissipated which leads to higher temperatures and greater movement. It's important to note that disregarding this phenomenon can cause weak thermo-magnetic simulations to overestimate high temperatures. The heat generation parameter is a standard for calculating the total thermal energy generated inside a fluid as a result of various processes, such as chemical reactions, friction, and outside energy sources. Heat generation within a fluid causes considerable temperature rises, which have a significant impact on the fluid's temperature. Fig. 4b shows that the parameter controlling heat generation improves fluid temperature. When compared to (AA7075-ethylene glycol), (AA7075-Ti-6Al-4 V/ethylene glycol) performs better. Physically, when a solar water heating system uses an electric pump to circulate water, this happens. Various parts of the system, including the pipes, present resistance to the flow of water. Due to friction, this resistance causes a portion of the object's kinetic energy to be converted into heat energy. Additionally, if the pump generates heat, which is frequently the case with electric pumps, this will add more thermal energy to the circulatory system.

6.3. Effect of suction ($S > 0$) and injection ($S < 0$)) on $\mathbf{f}'(\mathbf{\Gamma})$, $\boldsymbol{\theta}(\mathbf{\Gamma})$, and Ng for to (AA7075-Ti-6Al-4 V/ethylene glycol) HNF and (AA7075- ethylene glycol) NF

The parameters suction ($S > 0$) and injection ($S < 0$) is used in fluid mechanics to describe the flow of a fluid through a channel or pipe when suction or injection occurs at the wall. This parameter represents the relationship between suction and injection velocity at the wall and bulk velocity convection strength. An increase in wall velocity caused by suction can lead to heat transfer from the wall to the fluid, while injection reduces wall velocity and subsequently reduces heat transfer. Based on Fig. 5a and b, it is evident that higher values of ($S > 0$) result in a reduction in the velocity flow and thermal behavior. Elevation in the value of ($S > 0$) results in a rise in frictional resistance between the fluid and its surface, reducing the flow velocity. This phenomenon occurs due to the presence of numerous rough elements or irregularities on the surface when ($S > 0$) is high, which creates a greater hindrance for the fluid to overcome. Consequently, it moves at a slower pace and experiences reduced velocity. Both Fig. 5c and d ($S < 0$) increased the velocity of the fluid and thermal distribution. It was observed that the physical characteristics (AA7075- ethylene glycol) NF is higher than the (AA7075-Ti-6Al-4 V/ethylene glycol) HNF. Physically, when a considerable quantity of liquid is injected into the surface, it generates a high-pressure area where it is injected. This high pressure can lead to an acceleration in flow velocity as the fluid moves through the medium. The injection of copious amounts of liquid can create fissures or openings in the medium that were previously blocked. Consequently, this can increase permeability and subsequently increase flow velocity.

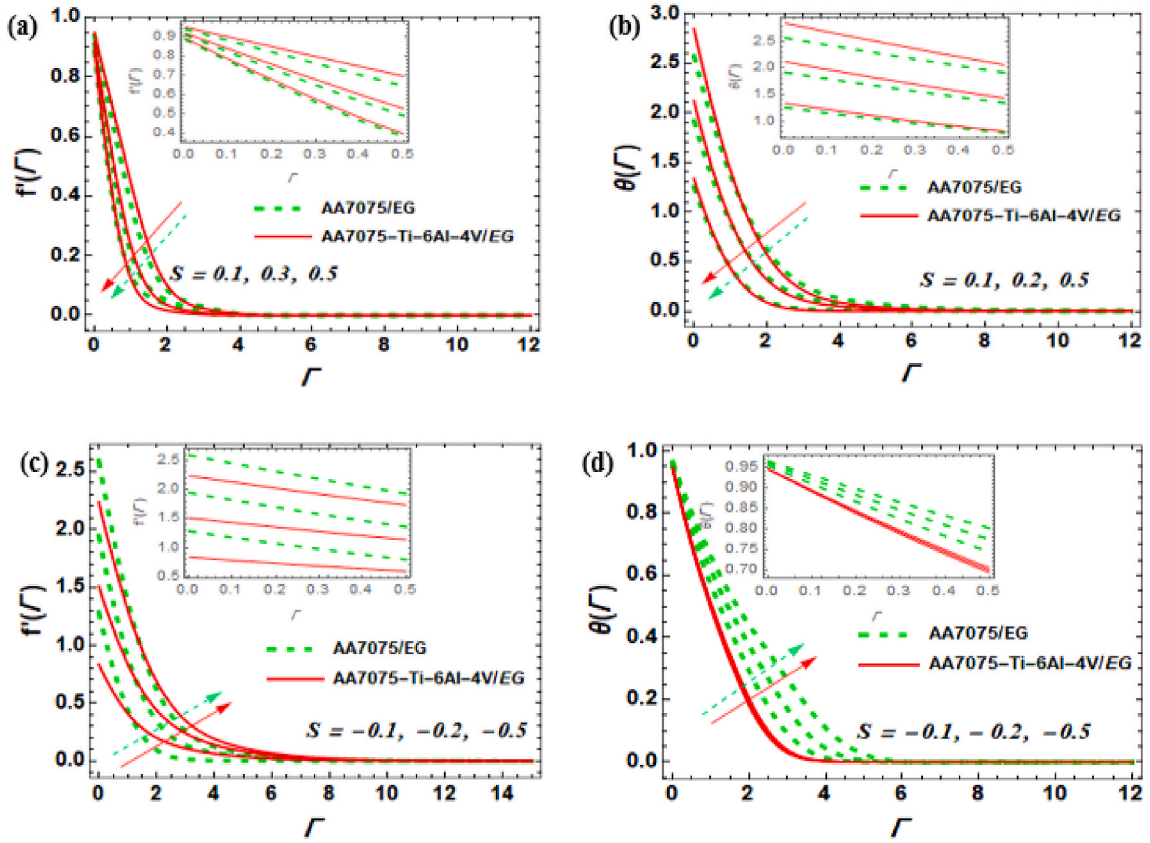

Fig. 5. Impact of $(S > 0)$ *and* $(S < 0)$ on $'(\Gamma)$, *and* $\theta(\Gamma)$.

6.4. Effect of Deborah number I (ϱ_1) and Deborah number II (ϱ_2) on f' (Γ), and $\theta(\Gamma)$ for (AA7075-Ti-6Al-4V/ethylene glycol) HNF and (AA7075- ethylene glycol) NF

The Deborah number is a rheology parameter that gives an insight into the flow behavior of materials in response to deformation. Its computation involves comparing the time taken for a material to recover its initial state after deformation with the time taken for the deformation. A higher value of the Deborah number indicates that the material has more elasticity and can recover its original shape quickly, whereas a lower value suggests that the material is more viscous and takes a longer time to return to its original shape after deformation. Consequently, it is necessary to consider the effects of Deborah's number on the system. The speed profile is affected by the ratio ϱ_1 between relaxation time and retardation time, as shown in Fig. 6a. As the value of *Deborah number I* (ϱ_1) increases, there is a simultaneous decrease in both retardation time and relaxation time. This indicates that when exposed to higher intensity, the substance reacts promptly and achieves its original state faster. Fig. 6b illustrates the impact of Deborah's number on temperature. It should be noted that an increase in χ resulted in a noticeable temperature rise. This occurrence arises from the impediment offered to the fluid flow, leading to its deceleration. Conversely, Fig. 6c displays the impact of different values of *Deborah number II* (ϱ_2). An increase in Deborah number results in a longer retardation time, which is illustrated in Fig. 6d and is dependent on the retardation time of Deborah number II (ϱ_2). This indicates that the strength of elasticity is technically enhanced by an increase in the retardation time of Deborah number II (ϱ_2). The interaction between elasticity and viscosity in fluids shows an inverse relationship. This means that as the viscosity decreases, the fluid velocity increases. In other words, when the Deborah number increases, it leads to a rise in velocity. It was observed that the physical characteristics (AA7075- ethylene glycol) NF is higher then the (AA7075-Ti-6Al-4 V/ethylene glycol) HNF (Fig. 6d).

6.5. Effect of velocity sli p δ on f′(Γ), and θ(Γ) for to (AA7075-Ti-6Al-4 V/ethylene glycol) HNF and (AA7075- ethylene glycol) NF

Slip velocity refers to the speed difference between a fluid and a surface in cases where there is a slip boundary condition or slippage at the point of contact. This term is typically used in the context of fluid mechanics to explain the movement of fluids near surfaces, particularly in situations such as solid-liquid interfaces or microfluidic devices. As the velocity slip decreases, it indicates a decrease in the relative difference between fluid and surface velocities. Consequently, there is a reduction in fluid flow velocity due to lowered shear stress at the surface, leading to less friction. Thus, there is an overall decrease in energy transfer from the fluid to its surrounding environment, resulting in reduced fluid velocity. It was observed that the (AA7075- ethylene glycol) NF is higher than (AA7075-Ti-6Al-4 V/ethylene glycol) (see Fig. 7a). Physically, in water pumping systems that rely on solar power, velocity slip plays a crucial role as it impacts system efficiency. When there is a significant amount of velocity slip, more energy is needed to overcome frictional losses, which in turn reduces the overall efficiency of the system. However, by decreasing the velocity slip, solar pumps can function more effectively and consume less energy, resulting in significant energy savings. Velocity slip refers to the relative movement between a fluid and a solid surface. This movement generates friction leading to an increase in the temperature of the fluid due to the heat generated from friction (see Fig. 7b). Essentially, energy is converted into heat due to the friction caused by the slip. This phenomenon

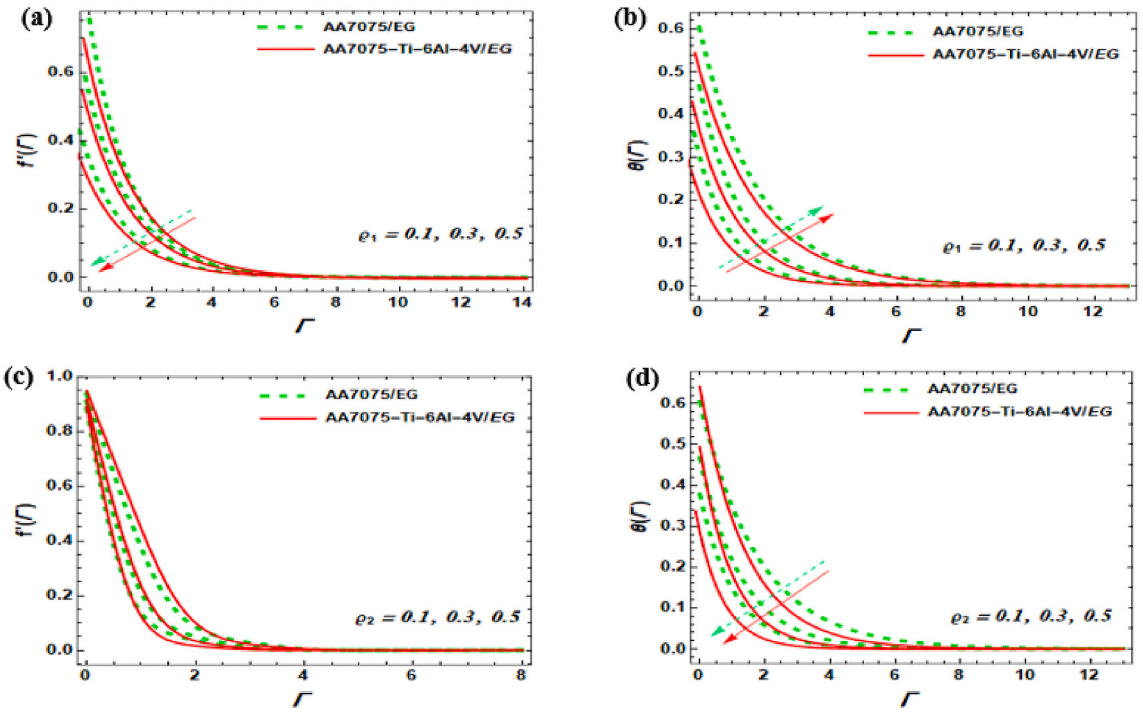

Fig. 6. Impact of ϱ_1 , *and* ϱ_2 on f '(Γ), and $\theta(\Gamma)$.

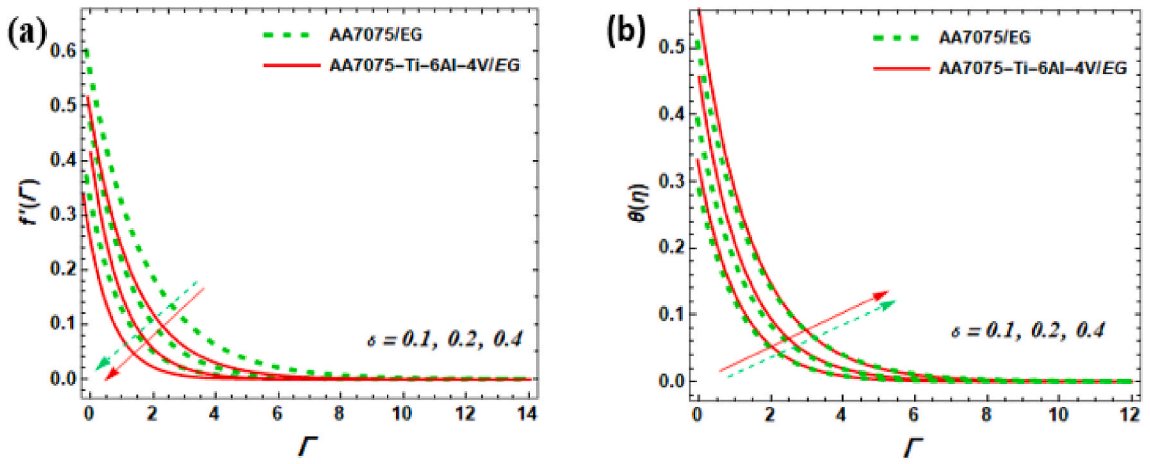

Fig. 7. Impact of δ on f '(Γ), and $\theta(\Gamma)$.

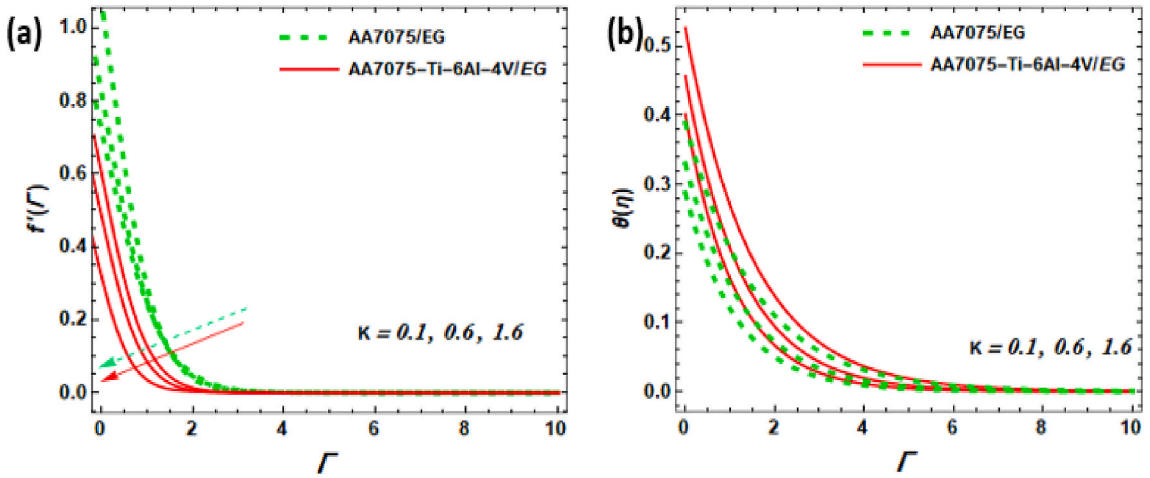

Fig. 8. Influence of K on f '(Γ), and $\theta(\Gamma)$.

is commonly observed in microfluidic systems where channels or confinement geometries are small enough for velocity slip to become significant.

6.6. *Effect of porous medium (K) on* $\dot{f}(\Gamma)$ *for (AA7075-Ti-6Al-4 V/ethylene glycol) HNF and (AA7075- ethylene glycol) NF*

Fig. 8a illustrates the porous medium that can be used to measure the flow velocity. According to the result, the porous medium has an impact on decreasing the velocity of the flow. When compared to (AA7075-ethylene glycol), (AA7075-Ti-6Al-4 V/ethylene glycol) behaves better. Physically, Darcy's law is a reliable way to measure the decrease in the speed of fluid through a porous material. This law explains how the flow rate and the pressure drop across the medium are related. Specifically, it states that as the pressure gradient increases, the flow rate also increases but this is inversely proportional to the permeability of the material. When a fluid passes through a porous medium, it needs to navigate through small channels. This decreases the cross-sectional area available for flow and increases the resistance to flow. As a result, the fluid velocity decreases. The use of porous media has other benefits as well, such as preventing damage to solar pump components that may be caused by high velocities or pressure in the system due to reduced fluid velocity. Besides this, using porous media can also increase the efficiency of solar pumps by reducing losses due to friction and turbulence in the system, leading to lower energy consumption and better overall performance. The fluid's temperature goes up due to the heat that is produced, which leads to more thermal energy being transferred from the porous medium to the fluid (see Fig. 8b). This process has practical applications in solar water heating systems that use solar pumps. The solar pump heats water by circulating it through a collector panel, where it absorbs the sun's heat. Using a porous medium such as sand or rocks within this system provides an extra source of heat transfer from the porous medium to the water, which increases its temperature further before being stored for later use. Therefore, incorporating a porous medium promotes efficiency by increasing the heating capacity and reducing reliance on gas- or electricity-powered heating elements in such systems.

6.7. Effect of Biot number (Bi) on $f'(\Gamma)$ for (AA7075-Ti-6Al-4V/ethylene glycol) HNF and (AA7075- ethylene glycol) NF

The Biot number (Bi) is a non-dimensional parameter that indicates how fast heat is conducted inside a solid material compared to how fast it is transferred across its surface by convection. It can be calculated by dividing the resistance of convective heat transfer by the resistance of conductive heat transfer. As the Biot number is greater than 1 (Bi $>$ 1), it means that heat transfer inside a solid is slower at its surface. The transfer of heat from a surface to a solid can cause heat to accumulate within the solid, which will increase its temperature. If there is fluid flowing through or over the solid, this increase in temperature can be transferred to the fluid and result in a higher temperature. The value of Bi becomes less than 1 (Bi $<$ 1), this leads to uniform temperature within the solid because any generated or lost heat at any point in the material will be quickly carried away by conduction through surrounding regions and then transferred via convection to the fluid around it, resulting in minimal differences in temperature across various parts of the solid. In addition, when equals infinity (Bi $<\infty$), there is an immediate transfer of heat at the fluid's surface. This happens when there is a high rate of convective or conductive heat transfer between the fluid and a solid interface. Essentially, any changes in temperature within the fluid will be instantly observed on its surface. This condition has significant implications for industrial and natural processes that involve fluids, such as cooling electronic devices and producing geothermal energy (see Fig. 9a). Furthermore, the behavior of Bi on entropy generation is displayed in Fig. 9b. This is illustrated through diagrams that depict a gradual increase in changes at the surface. Additionally, there appears to be minimal improvement toward the stretched walls.

6.8. Effect of nanoparticle volume friction (φ, φ_h) on $f'(\Gamma)$, and $\theta(\Gamma)$ for (AA7075-Ti-6Al-4V/ethylene glycol) HNF and (AA7075- ethylene glycol) NF

The presence of nanoparticles in a fluid has a significant impact on its physical properties such as fluid flow and thermal distribution. The size of nanoparticles is a crucial factor that affects five quantities, represented by the $\omega_1 = (1-(\varphi_1+\varphi_2))^{2.5}, \omega_2 = (1-(\varphi_1+\varphi_2)) + \varphi_1\rho_{s_1}/\rho_f + \varphi_2\rho_{s_2}/\rho_f$, $\omega_3 = (1-(\varphi_1+\varphi_2)) + \varphi_1(\rho C_p)_{s1}/(\rho C_p)_f + \varphi_2(\rho C_p)_{s2}/(\rho C_p)_f$, $\omega_4 = \left(\frac{(k_{s2}+2k_{nf}-2\varphi_2(k_{nf}-k_{s2})}{(k_{s2}+2k_{nf}+\varphi_2(k_{nf}-k_{s2})}\right) \times \left(\frac{k_{s1}+2k_f-2\varphi_1(k_f-k_{s1})}{(k_{s1}+2k_f+\varphi_1(k_f-k_{s1})}\right)$ based on the Tiwari-Das nanoscale model. The introduction of nanoparticles into a fluid can result in volume friction that hinders the velocity profile. As viscosity measures the ease with which fluids flow, adding nanoparticles creates additional friction by interacting with fluid molecules, ultimately impeding fluid motion. Consequently, this increases. The introduction of nanoparticles into a fluid can lead to volume friction that impacts the velocity profile. Viscosity, which is a measure of fluid flowability, is affected by interactions between the nanoparticles and fluid molecules. These interactions increase friction, making it harder for the fluid to flow and leading to higher viscosity and lower flow rate. The AA7075-Ti-6Al-4 V/ethylene glycol composite exhibits a significant enhancement in its velocity when the nanostructure size is reduced (see Fig. 10a). Thus, it can be inferred that the optimal dispersion of nano molecules is achieved when their size is sufficiently small. Additionally, as seen in Fig. 10b, the size of the nanoparticles plays a significant role in thermal distribution within the fluid. When the size of nano molecules decreases, they tend to diffuse further in the far-field flow due to temperature differences. As a result, the thickness of the thermal boundary layer increases. By determining the minimum size threshold for nano molecules that can still produce a satisfactory temperature profile, we can achieve optimal results. When compared to (AA7075-Ti-6Al-4V/ethylene glycol), (AA7075-Ti-6Al-4 V/ethylene glycol) performs better.

6.9. Impact Reynolds number (Re) and Brinkman number (Br) for (AA7075-Ti-6Al-4V/ethylene glycol) HNF and (AA7075- ethylene glycol) NF

The mathematical simulation of irreversible energy losses involves the production of entropy, and the objective of the research is to discover strategies to reduce the pace at which this phenomenon takes place. For us to accomplish this objective, we first need to locate the elements that have a propensity to increase the entropy, and then we must devise solutions that would slow down that pace. It is crucial to highlight Re effectiveness in facilitating fluid flow. Fig. 11a depicts the intensified impact on entropy production, indicating an improvement in efficiency. Hence, in a fluid flow system, raising the Reynolds number can potentially escalate the level of turbulence intensity. This is further expected to result in a surge in the generation of entropy. In fluid mechanics, the Brinkman number (Br) is a non-dimensional value that characterizes the significance of viscous forces and Darcy's law, which relates the flow rate of fluid to the pressure gradient. On the other hand, entropy generation pertains to the quantity of energy dissipated caused by irreversibilities within a system, such as heat transfer through a finite temperature difference or fluid movement through porous media. The Brinkman number has a crucial role in determining the amount of entropy generated, which can be explained by the ratio of viscous forces to inertia forces present in a porous medium. If the value of Br is low, then there will be a laminar flow with minimal entropy generation because viscous forces would exceed inertia forces. However, if the value of Br is high, then turbulence may occur due to significant inertia forces resulting in an increased level of entropy generation due to less efficient transfer of energy and more mixing (see Fig. 11b).

7. Conclusions

The present study aims to examine the applications of solar energy in water pumping systems and entropy generation minimization for Oldroyd-b (AA7075-Ti-6Al-4V/ethylene glycol) HNF and (AA7075- ethylene glycol) NF. The research analyzed several control factors that affect the extended straight flat exterior on SWP, including Deborah number, radiation, Eckert number, and suction/injection, Biot number, and porous medium. The results were presented through tables and figures and the main purpose was to enhance the energy efficiency of the SWP.

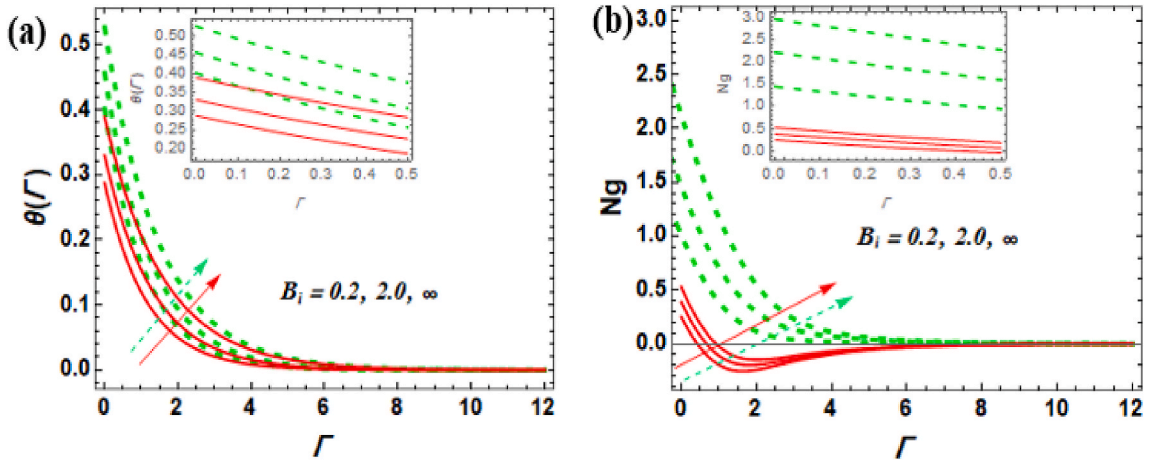

Fig. 9. Influence of Bi on θ(Γ), and Ng.

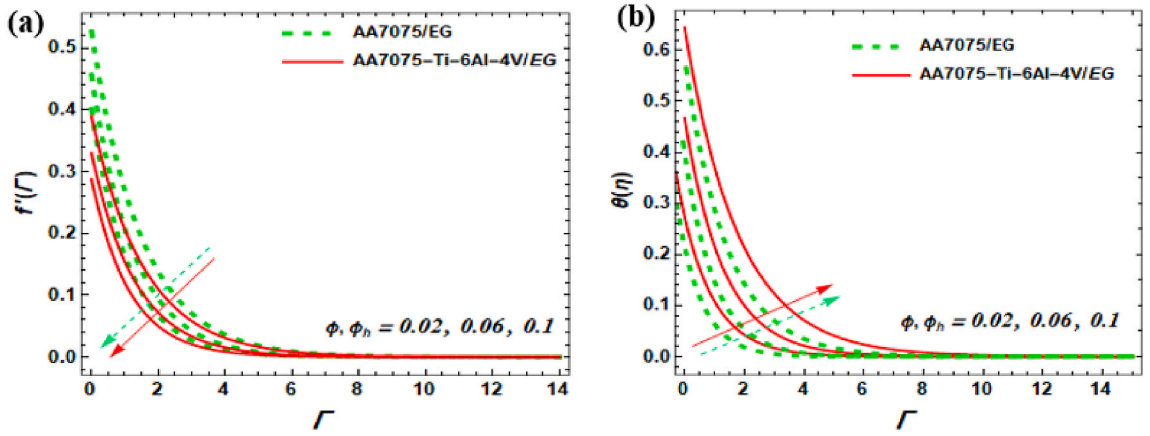

Fig. 10. Effect of φ, φ_h on f '(Γ), and $\theta(\Gamma)$.

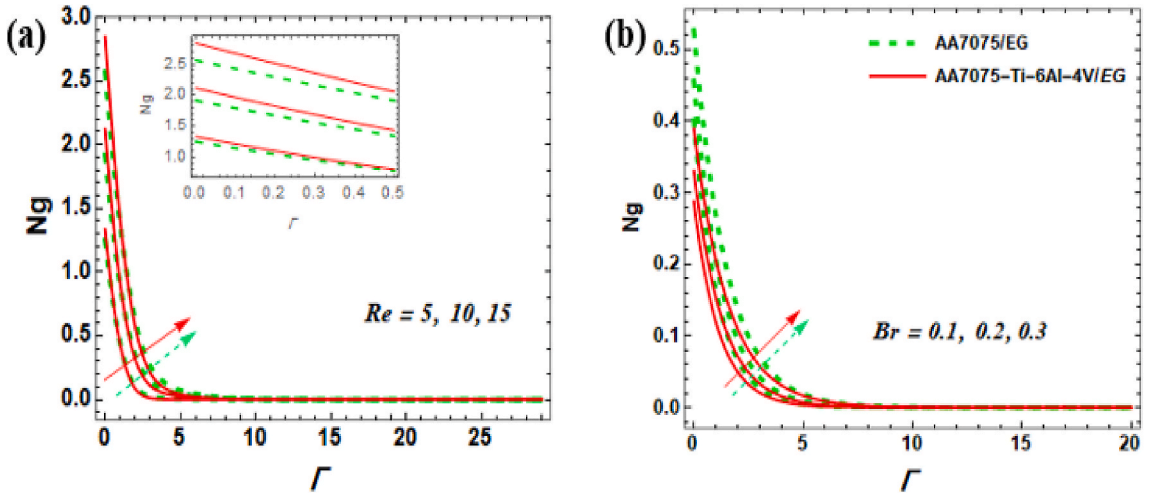

Fig. 11. Effect of *Br and, Re* on Ng.

- The study has found that the Ec for (AA7075-ethylene glycol) is a more effective thermal conductor compared to the (AA7075-Ti-6Al-4V/ethylene glycol). This emphasizes the potential for using AA7075-Ti-6Al-4V/ethylene glycol in thermal management applications where high levels of heat transfer are required.
- The result shows that an increase in the values of Deborah number II and injection ($S < 0$) increase the velocity profiles, while an increase in Porous medium, Deborah number I, and velocity sli p leads to a decrease in velocity profiles.
- The combination of AA7075-Ti-6Al-4V/ethylene glycol hybrid nanofluid leads to better thermal radiative performance compared to the AA7075-ethylene glycol nanofluid.
- The factors that contributed to improved heat transfer are thermal radiation, heat generation, Deborah number I, and Deborah number II, injection ($S < 0$), Biot number, velocity sli p, and nanoparticle volume fraction.
- The Galerkin Weighted Residual Method produces a set of converging solutions for this problem, based on the physical parameter values used.

Furthermore, The results indicate that using an (AA7075-Ti-6Al-4V/ethylene glycol) HNF and (AA7075- ethylene glycol) NF in PTSC through an extended straight fat exterior can considerably enhance the thermal efficiency of SWP. Therefore, it can be inferred that the utilization of these nanofluids holds the potential for improving the performance of SWP. Utilizing HNF has been found to result in superior thermal radiative enhancement compared to traditional NF. Additionally, the Galerkin Weighted Residual Method has proven to be a precise and effective model for analyzing fluid flow. The study highlights the significance of certain factors, including Reynolds number, thermal radiation, and Brinkman number, in managing entropy generation. This emphasizes the importance of controlling these parameters to manage entropy generation effectively. The study's findings indicate a noteworthy enhancement in thermal efficiency which could result in substantial cost reduction and positive environmental impact for the development and management of water pumps powered by solar energy.

8. Future direction

Based on the current research, it is recommended to explore further the use of parabolic trough surface collector (PTSC) installation models for solar water pumps (SWP). As solar radiation is crucial for the operation of photovoltaic cells and SWP, continued efforts should be made to improve the efficacy of SWP.

Future studies could focus on measuring thermal transmission proportions of different warmth transmission liquids in PTSC, including hybrid nano-fluids, and comparing their performance. Additionally, further testing could be conducted using modified Buongiorno's model to analyze entropy analysis of Oldroyd-B hybrid nano-fluids.

These findings have the potential to enhance the efficiency and sustainability of SWP systems, playing a crucial role in granting clean water access to various regions globally.

Author's contribution Statement

A.M. Obalalu, A. Abbas: Conceptualization, Methodology, Software, Validation; data curation; Formal analysis, Writing – original draft. **M. Asif Memon:** Writing–original draft, software, Investigation, Validation. **S. Saleem:** Writing–review & editing, Data curation, Visualization. **O. A Olayemi:** Validation, Investigation, Writing–review & editing, Formal analysis. **Mohamed R. Ali:** Methodology, Formal analysis, Supervision, Funding. **R. Sadat, A.S. Hendy:** provided significant feedback and assisted in the revised version of manuscript. Further, they have also assisted us in revising the manuscript critically for important intellectual content

Declaration of Competing interest

The authors declare that they have no known competing financial interests or personal relationships that could have appeared to influence the work reported in this paper.

Acknowledgments

The authors extend their appreciation to the Deanship of Scientific Research at King Khalid University for funding this work through research groups program under Grant No. R.G.P2/115/44.

Data availability

No data was used for the research described in the article.

References

[1] H.K. Gupta, G.D. Agrawal, J. Mathur, Investigations for effect of Al2O3–H2O nanofluid flow rate on the efficiency of direct absorption solar collector, Case Stud. Therm. Eng. 5 (2015) 70–78.
[2] G. Alimonti, L. Mariani, F. Prodi, R.A. Ricci, A critical assessment of extreme events trends in times of global warming, Eur. Phys. J. Plus 137 (2022) 1–20.
[3] K. Lan, S.S. Kelley, P. Nepal, Y. Yao, Dynamic life cycle carbon and energy analysis for cross-laminated timber in the Southeastern United States, Environ. Res. Lett. 15 (2020), 124036.
[4] P. Nejat, F. Jomehzadeh, M.M. Taheri, M. Gohari, M.Z.A. Majid, A global review of energy consumption, CO2 emissions and policy in the residential sector (with an overview of the top ten CO2 emitting countries), Renew. Sustain. Energy Rev. 43 (2015) 843–862.
[5] F.A. Wahaab, L.L. Adebayo, A.A. Adekoya, J.Y. Yusuf, A.M. Obalalu, A.O. Yusuff, B. Alqasem, Electromagnetic wave-induced nanofluid-oil interfacial tension reduction for enhanced oil recovery, J. Mol. Liq. 318 (2020), 114378.

[6] A.M. Obalalu, S.O. Salawu, O.A. Olayemi, O.A. Ajala, K. Issa, Analysis of hydromagnetic Williamson fluid flow over an inclined stretching sheet with Hall current using Galerkin Weighted Residual Method, Comput. Math. Appl. 146 (2023) 22–32.
[7] S. Gorjian, H. Ebadi, M. Trommsdorff, H. Sharon, M. Demant, S. Schindele, The advent of modern solar-powered electric agricultural machinery: a solution for sustainable farm operations, J. Clean. Prod. 292 (2021), 126030.
[8] G.V. Ochoa, M.V. Chamorro, O.C. Silvera, Thermo-economic and sustainability assessment of two solar organic Rankine cycles in the United States, Sustain. Energy Technol. Assessments 50 (2022), 101758.
[9] A.A. Minea, W.M. El-Maghlany, Influence of hybrid nanofluids on the performance of parabolic trough collectors in solar thermal systems: recent findings and numerical comparison, Renew. Energy 120 (2018) 350–364.
[10] A. Obalalu, T. Oreyeni, A. Abbas, M.A. Memon, U. Khan, E.-S.M. Sherif, A.M. Hassan, I. Pop, Implication of electromagnetohydrodynamic and heat transfer analysis in nanomaterial flow over a stretched surface: applications in solar energy, Case Stud. Therm. Eng. (2023), 103381.
[11] T. Short, R. Oldach, Solar powered water pumps: the past, the present—and the future? J. Sol. Energy Eng. 125 (2003) 76–82.
[12] zN. Stupnitska, E. Sribna, Historical Aspects Of Solar Energy In The World, Economics, Management, Law: Problems Of Establishing And Transformation, 2016, pp. 33–35.
[13] S. Salawu, A. Obalalu, E. Fatunmbi, R. Oderinu, Thermal Prandtl-Eyring hybridized MoS2-SiO2/C3H8O2 and SiO2-C3H8O2 nanofluids for effective solar energy absorber and entropy optimization: a solar water pump implementation, J. Mol. Liq. 361 (2022), 119608.
[14] J. Xu, J. Zhang, K. Kuang, J. Xu, J. Zhang, K. Kuang, Manufacturing Solar Cells: Assembly and Packaging, Conveyor Belt Furnace Thermal Processing, 2018, pp. 35–41.
[15] C.E. Fritts, On the Fritts selenium cells and batteries, J. Franklin Inst. 119 (1885) 221–232.
[16] W. Jamshed, N.A.A.M. Nasir, S.S.P.M. Isa, R. Safdar, F. Shahzad, K.S. Nisar, M.R. Eid, A.-H. Abdel-Aty, I. Yahia, Thermal growth in solar water pump using Prandtl–Eyring hybrid nanofluid: a solar energy application, Sci. Rep. 11 (2021) 1–21.
[17] A. Obalalu, M.A. Memon, O. Olayemi, J. Olilima, A. Fenta, Enhancing heat transfer in solar-powered ships: a study on hybrid nanofluids with carbon nanotubes and their application in parabolic trough solar collectors with electromagnetic controls, Sci. Rep. 13 (2023) 9476.
[18] X. Zhu, Z. Guo, Z. Hou, Solar-powered airplanes: a historical perspective and future challenges, Prog. Aero. Sci. 71 (2014) 36–53.
[19] A. Obalalu, H. Ahmad, S. Salawu, O. Olayemi, C. Odetunde, A. Ajala, A. Abdulraheem, Improvement of Mechanical Energy Using Thermal Efficiency of Hybrid Nanofluid on Solar Aircraft Wings: an Application of Renewable, Sustainable Energy, Waves in Random Complex Media, 2023, pp. 1–30.
[20] S. Chandrasekaran, M. Satyanarayana Gupta, S. Jangid, K. Loganathan, B. Deepa, D.K. Chaudhary, Unsteady radiative Maxwell fluid flow over an expanding sheet with sodium alginate water-based copper-graphene oxide hybrid nanomaterial: an application to solar aircraft, Adv. Mater. Sci. Eng. (2022) 2022.
[21] I. Ullah, T. Hayat, A. Alsaedi, Optimization of entropy production in flow of hybrid nanomaterials through Darcy–Forchheimer porous space, J. Therm. Anal. Calorim. 147 (2022) 5855–5864.
[22] T. Zubair, M. Usman, K.S. Nisar, I. Khan, H. Zahran, A.H. Almaliki, Numerical assessment of heat and mass transportation in […formula…], in: Nanofluids Influenced by Soret and Dufour Effects, vol. 12, Scientific Reports, 2022.
[23] M. Rezaeian, M.S. Dehaj, M.Z. Mohiabadi, M. Salarmofrad, S. Shamsi, Experimental investigation into a parabolic solar collector with direct flow evacuated tube, Appl. Therm. Eng. 189 (2021), 116608.
[24] Z. Said, M. Ghodbane, B. Boumeddane, A.K. Tiwari, L.S. Sundar, C. Li, N. Aslfattahi, E. Bellos, S. Cells, Energy, exergy, economic and environmental (4E) analysis of a parabolic trough solar collector using MXene based silicone oil nanofluids, Sol. Energy Mater. 239 (2022), 111633.
[25] W. Ibrahim, Magnetohydrodynamics (MHD) flow of a tangent hyperbolic fluid with nanoparticles past a stretching sheet with second order slip and convective boundary condition, Results Phys. 7 (2017) 3723–3731.
[26] O.A. Olayemi, A.M. Obalalu, C.B. Odetunde, O.A. Ajala, Heat transfer enhancement of magnetized nanofluid flow due to a stretchable rotating disk with variable thermophysical properties effects, Eur. Phys. J. Plus 137 (2022) 1–12.
[27] W. Jamshed, M.R. Eid, F. Shahzad, R. Safdar, M. Shamshuddin, Keller Box Analysis for Thermal Efficiency of Magneto Time-dependent Nanofluid Flowing in Solar-Powered Tractor Application Applying Nano-Metal Shaped Factor, Waves in Random Complex Media, 2022, pp. 1–36.
[28] H. Waqas, M. Fida, D. Liu, U. Manzoor, T. Muhammad, Numerical simulation of entropy generation for nanofluid with the consequences of thermal radiation and Cattaneo-Christov heat flux model, Int. Commun. Heat Mass Tran. 137 (2022), 106293.
[29] J. Shah, F. Ali, N. Khan, Z. Ahmad, S. Murtaza, I. Khan, O. Mahmoud, MHD flow of time- fractional Casson nanofluid using generalized Fourier and Fick's laws over an inclined channel with applications of gold nanoparticles, Sci. Rep. 12 (2022), 17364.
[30] S. Murtaza, P. Kumam, Z. Ahmad, T. Seangwattana, I.E. Ali, Numerical analysis of newly developed fractal-fractional model of Casson fluid with exponential memory, Fractals 30 (2022), 2240151.
[31] S. Murtaza, Z. Ahmad, I.E. Ali, Z. Akhtar, F. Tchier, H. Ahmad, S.-W. Yao, Analysis and numerical simulation of fractal-fractional order non-linear couple stress nanofluid with cadmium telluride nanoparticles, J. King Saud Univ. Sci. 35 (2023), 102618.
[32] S. Murtaza, P. Kumam, M. Bilal, T. Sutthibutpong, N. Rujisamphan, Z. Ahmad, Parametric simulation of hybrid nanofluid flow consisting of cobalt ferrite nanoparticles with second- order slip and variable viscosity over an extending surface, Nanotechnol. Rev. 12 (2023), 20220533.
[33] L.O. Ajuka, M.K. Odunfa, M.O. Oyewola, O.M. Ikumapayi, S.A. Akinlabi, E.T. Akinlabi, Modeling of viscosity of composite of TiO2–Al2O3 and ethylene glycol nanofluid by artificial neural network: experimental correlation, Int. J. Interact. Des. Manuf. (2022) 1–10.
[34] S. Salawu, A. Obalalu, E. Fatunmbi, A. Disu, N. Akkurt, Magneto-couple Stress of Tri- Hybrid Metallic Oxide Nanomaterials in Porous Media with Nonlinear Properties for Thermal Technology Advancement, Scientific African, 2023, e01841.
[35] T. Hayat, S. Nadeem, A. Khan, Rotating flow of Ag-CuO/H 2 O hybrid nanofluid with radiation and partial slip boundary effects, Eur. Phys. J. E: Soft Matter Biol. Phys. 41 (2018) 1–9.
[36] H. Rajabi-Moghaddam, M. Naimi-Jamal, M. Tajbakhsh, Fabrication of copper (II)-coated magnetic core-shell nanoparticles Fe3O4@ SiO2-2-aminobenzohydrazide and investigation of its catalytic application in the synthesis of 1, 2, 3-triazole compounds, Sci. Rep. 11 (2021) 1–14.
[37] N. Abed, I. Afgan, A. Cioncolini, H. Iacovides, A. Nasser, T. Mekhail, Thermal performance evaluation of various nanofluids with non-uniform heating for parabolic trough collectors, Case Stud. Therm. Eng. 22 (2020), 100769.
[38] F.L. Rashid, A. Hadi, N.H. Al-Garah, A. Hashim, Novel phase change materials, MgO nanoparticles, and water based nanofluids for thermal energy storage and biomedical applications, Int. J. Pharm. Phytopharmacol. Res. 8 (2018) 46–56.
[39] M.A. Qureshi, A case study of MHD driven Prandtl-Eyring hybrid nanofluid flow over a stretching sheet with thermal jump conditions, Case Stud. Therm. Eng. 28 (2021), 101581.
[40] A. Aziz, W. Jamshed, T. Aziz, H.M. Bahaidarah, K. Ur Rehman, Entropy analysis of Powell–Eyring hybrid nanofluid including effect of linear thermal radiation and viscous dissipation, J. Therm. Anal. Calorim. 143 (2021) 1331–1343.
[41] T. Sajid, W. Jamshed, R. Safdar, S.M. Hussain, F. Shahzad, M. Bilal, Z. Rehman, M.M. Rahman, A.A. Pasha, Features and aspects of radioactive flow and slippage velocity on rotating two-phase Prandtl nanofluid with zero mass fluxing and convective constraints, Int. Commun. Heat Mass Tran. 136 (2022), 106180.
[42] S.M. Hussain, Thermal-Enhanced Hybrid of Copper–Zirconium Dioxide/ethylene Glycol Nanofluid Flowing in the Solar Collector of Water-Pump Application, Waves in Random Complex Media, 2022, pp. 1–28.
[43] F. Shahzad, W. Jamshed, R. Safdar, S.M. Hussain, N.A.A.M. Nasir, M. Dhange, K.S. Nisar, M.R. Eid, M. Sohail, M. Alsehli, Thermal analysis characterisation of solar-powered ship using Oldroyd hybrid nanofluids in parabolic trough solar collector: an optimal thermal application, Nanotechnol. Rev. 11 (2022) 2015–2037.
[44] S.M. Hussain, Irreversibility Analysis of Time-dependent Magnetically Driven Flow of Sutterby Hybrid Nanofluid: a Thermal Mathematical Model, Waves in Random Complex Media, 2022, pp. 1–33.
[45] S. Parvin, S.S.P.M. Isa, F.S. Al-Duais, S.M. Hussain, W. Jamshed, R. Safdar, M.R. Eid, The flow, thermal and mass properties of Soret-Dufour model of magnetized Maxwell nanofluid flow over a shrinkage inclined surface, PLoS One 17 (2022), e0267148.

[46] S.M. Hussain, Dynamics of ethylene glycol-based graphene and molybdenum disulfide hybrid nanofluid over a stretchable surface with slip conditions, Sci. Rep. 12 (2022) 1751.
[47] S.M. Hussain, W. Jamshed, M.R. Eid, Solar-HVAC thermal investigation utilizing (Cu- AA7075/C6H9NaO7) MHD-driven hybrid nanofluid rotating flow via second-order convergent technique: a novel engineering study, Arabian J. Sci. Eng. 48 (2023) 3301–3322.
[48] S.M. El Din, A. Darvesh, A. Ayub, T. Sajid, W. Jamshed, M.R. Eid, S.M. Hussain, M. Sánchez-Chero, S.M. Ancca, J.M. Ramírez Cerna, Quadratic multiple regression model and spectral relaxation approach for carreau nanofluid inclined magnetized dipole along stagnation point geometry, Sci. Rep. 12 (2022), 17337.
[49] A. Belhadj Mahammed, R. Fares, M. Lounis, W. Jamshed, S.M. Hussain, M.R. Eid, Thermal management of magnetohydrodynamic nanofluid within porous C-shaped cavity with undulated baffle, J. Thermophys. Heat Tran. 36 (2022) 594–611.
[50] A.A. Khan, M.N. Khan, S. Nadeem, S.M. Hussain, M. Ashraf, Part E: Journal of Process Mechanical Engineering, Thermal Slip and Homogeneous/Heterogeneous Reaction Characteristics of Second-Grade Fluid Flow over an Exponentially Stretching Sheet, 2021, 09544089211064187.
[51] A.M. Obalalu, L.L. Adebayo, I. Colak, A.O. Ajala, F.A. Wahaab, Entropy generation minimization on electromagnetohydrodynamic radiative Casson nanofluid flow over a melting Riga plate, Heat Transfer 51 (5) (2022) 3951–3978.
[52] zA.M. Obalalu, A.O. Ajala, A.O. Akindele, O.A. Areo, S.D. Ogundiran, K.A. Salaudeen, S. Alao, Entropy Generation Minimization for Radiative Casson Fluid Flow through Permeable Walls and Convective Heating: A Comprehensive Numerical Investigation, Defect and Diffusion Forum, Trans Tech Publ, 2022, pp. 21–38.
[53] S. Salawu, A. Obalalu, E. Fatunmbi, M. Shamshuddin, Elastic deformation of thermal radiative and convective hybrid SWCNT-Ag and MWCNT-MoS4 magneto-nanofluids flow in a cylinder, Results Mater. (2023), 100380.
[54] A. Bejan, Maximum power from fluid flow, Int. J. Heat Mass Tran. 39 (1996) 1175–1181.
[55] A. Bejan, Constructal theory: from thermodynamic and geometric optimization to predicting shape in nature, Energy Convers. Manag. 39 (1998) 1705–1718.
[56] R. Agrawal, P. Kaswan, Entropy generation minimization of Ag-Fe_3O_4/water-ethylene glycol squeezed hybrid nanofluid flow between parallel disks, Int. J. Numer. Methods Heat Fluid Flow 33 (2023) 65–95.
[57] S. Ahmad, Z.H. Khan, S. Zeb, M. Hamid, Thermal and Entropy generation analysis of magnetohydrodynamic tangent hyperbolic slip flow towards a stretching sheet, Proc. IME E J. Process Mech. Eng. 236 (2022) 357–367.
[58] F. Shahzad, W. Jamshed, M.R. Eid, R. Safdar, S.S. Putri Mohamed Isa, S.M. El Din, N.A.A. Mohd Nasir, A. Iqbal, Thermal cooling efficacy of a solar water pump using Oldroyd-B (aluminum alloy-titanium alloy/engine oil) hybrid nanofluid by applying new version for the model of Buongiorno, Sci. Rep. 12 (2022), 19817.
[59] A. Obalalu, S. Salawu, M.A. Memon, O. Olayemi, M.R. Ali, R. Sadat, C. Odetunde, O. Ajala, A. Akindele, Computational study of Cattaneo–Christov heat flux on cylindrical surfaces using CNT hybrid nanofluids: a solar-powered ship implementation, Case Stud. Therm. Eng. 45 (2023), 102959.
[60] S. Salawu, A. Obalalu, M. Shamshuddin, Nonlinear solar thermal radiation efficiency and energy optimization for magnetized hybrid Prandtl–eyring nanoliquid in aircraft, Arabian J. Sci. Eng. (2022) 1–12.
[61] U. Khan, A. Zaib, A. Ishak, S. Bakar, Time-dependent Blasius–Rayleigh–Stokes flow conveying hybrid nanofluid and heat transfer induced by non-fourier heat flux and transitive magnetic field, Case Stud. Therm. Eng. (2021), 101151.
[62] J. Ballor, T. Li, F. Prima, C.J. Boehlert, A. Devaraj, A review of the metastable omega phase in beta titanium alloys: the phase transformation mechanisms and its effect on mechanical properties, Int. Mater. Rev. 68 (2023) 26–45.
[63] V. Khanna, V. Kumar, S.A. Bansal, C. Prakash, M. Ubaidullah, S.F. Shaikh, A. Pramanik, A. Basak, S. Shankar, Fabrication of efficient aluminium/graphene nanosheets (Al-GNP) composite by powder metallurgy for strength applications, J. Mater. Res. Technol. 22 (2023) 3402–3412.
[64] A.M. Obalalu, A.O. Ajala, A.O. Akindele, O.A. Oladapo, O.O. Akintayo, O.M. Jimoh, Computational study of magneto-convective non-Newtonian nanofluid slip flow over a stretching/shrinking sheet embedded in a porous medium, Comput. Math. Appl. 4 (2022) 123–128.
[65] W. Ashraf Adnan, Thermal Efficiency in Hybrid (Al2O3-CuO/H2O) and Ternary Hybrid Nanofluids (Al2O3-CuO-Cu/H2O) by Considering the Novel Effects of Imposed Magnetic Field and Convective Heat Condition, Waves in Random Complex Media, 2022, pp. 1–16.
[66] M.M. Azim, A. Arifutzzaman, R. Saidur, M. Khandaker, D. Bradley, Recent Progress in Emerging Hybrid Nanomaterials towards the Energy Storage and Heat Transfer Applications: A Review, Journal of Molecular Liquids, 2022, 119443.
[67] A.M. Obalalu, Heat and mass transfer in an unsteady squeezed Casson fluid flow with novel thermophysical properties: analytical and numerical solution, Heat Transfer 50 (2021) 7988–8011.
[68] K. Loganathan, S. Rajan, An entropy approach of Williamson nanofluid flow with Joule heating and zero nanoparticle mass flux, J. Therm. Anal. Calorim. 141 (2020) 2599–2612.
[69] S.M. Hussain, Entropy generation and thermal performance of Williamson hybrid nanofluid flow used in solar aircraft application as the main coolant in parabolic trough solar collector. Waves Random Complex Media, 2023, pp. 1–34.
[70] A. Ishak, R. Nazar, I. Pop, Mixed convection on the stagnation point flow toward a vertical, continuously stretching sheet, J. Heat Tran. (2007) 129.
[71] S. Das, S. Chakraborty, R. Jana, O. Makinde, Entropy analysis of unsteady magneto- nanofluid flow past accelerating stretching sheet with convective boundary condition 36 (2015) 1593–1610.
[72] A. Ishak, R. Nazar, I. Pop, Boundary layer flow and heat transfer over an unsteady stretching vertical surface, Meccanica 44 (2009) 369–375.
[73] W. Jamshed, S. Uma Devi S, R. Safdar, F. Redouane, K.S. Nisar, M.R. Eid, Comprehensive analysis on copper-iron (II, III)/oxide-engine oil Casson nanofluid flowing and thermal features in parabolic trough solar collector, J. Taibah Univ. Sci. 15 (2021) 619–636.